Quantum frequency translation by four-wave mixing in a fiber: low-conversion regime.

Andersen, Lasse Mejling; McKinstrie, C. J.; Raymer, M. G.; Rottwitt, Karsten

Published in:
Optics Express

Link to article, DOI:
10.1364/OE.20.008367

Publication date:
2012

Document Version
Publisher's PDF, also known as Version of record

Quantum frequency translation by four-wave mixing in a fiber: low-conversion regime

L. Mejling,[1,*] **C. J. McKinstrie,**[2] **M. G. Raymer,**[3] **and K. Rottwitt**[1]

[1]*Department of Photonics Engineering, Technical University of Denmark, DK-2800 Kgs. Lyngby, Denmark*
[2]*Bell Laboratories, Alcatel-Lucent, Holmdel, New Jersey 07733, USA*
[3]*Department of Physics, University of Oregon, Eugene, Oregon 97403, USA*
**lman@fotonik.dtu.dk*

Abstract: In this paper we consider frequency translation enabled by Bragg scattering, a four-wave mixing process. First we introduce the theoretical background of the Green function formalism and the Schmidt decomposition. Next the Green functions for the low-conversion regime are derived perturbatively in the frequency domain, using the methods developed for three-wave mixing, then transformed to the time domain. These results are also derived and verified using an alternative time-domain method, the results of which are more general. For the first time we include the effects of convecting pumps, a more realistic assumption, and show that separability and arbitrary reshaping is possible. This is confirmed numerically for Gaussian pumps as well as higher-order Hermite-Gaussian pumps.

OCIS codes: (060.4370) Nonlinear optics, fibers; (190.4380) Nonlinear optics, four-wave mixing; (270.5585) Quantum information and processing.

References and links

1. S. Tanzilli, W. Tittel, M. Halder, O. Alibart, P. Baldi, N. Gisin, and H. Zbinden, "A photonic quantum information interface," Nature (London) **437**, 116–120 (2005).
2. H. J. Kimble, "The quantum internet," Nature (London) **453**, 1023–1030 (2008).
3. C. K. Hong, Z. Y. Ou, and L. Mandel, "Measurement of subpicosecond time intervals between two photons by interference," Phys. Rev. Lett. **59**, 2044–2046 (1987).
4. E. Knill, R. Laflamme, and G. J. Milburn, "A scheme for efficient quantum computation with linear optics," Nature (London) **409**, 46–52 (2001).
5. I. A. Walmsley and M. G. Raymer, "Toward quantum-information processing with photons," Science **307**, 1733–1734 (2005).
6. A. Ferraro, M. G. A. Paris, M. Bondani, A. Allevi, E. Puddu, and A. Andreoni. "Three-mode entanglement by interlinked nonlinear interactions in optical $\chi(2)$ media," J. Opt. Soc. Am. B **21**, 1241–1249 (2004).
7. A. V. Rodionov and A. S. Chirkin, "Entangled photon states in consecutive nonlinear optical interactions," JETP Lett. **79**, 253–256 and 582 (2004).
8. O. Pfister, S. Feng, G. Jennings, R. C. Pooser, and D. Xie, "Multipartite continuous-variable entanglement from concurrent nonlinearities," Phys. Rev. A **70**, 020302 (2004).
9. R. C. Pooser and O. Pfister, "Observation of triply coincident nonlinearities in periodically poled KTiOPO4," Opt. Lett. **30**, 2635–2637 (2005).
10. A. S. Villar, M. Martinelli, C. Fabre, and P. Nussenzveig, "Direct production of tripartite pump-signal-idler entanglement in the above-threshold optical parametric oscillator," Phys. Rev. Lett. **97**, 140504 (2006).
11. K. N. Cassemiro, A. S. Villar, P. Valente, M. Martinelli, and P. Nussenzveig, "Experimental observation of three-color optical quantum correlations," Opt. Lett. **32**, 695–697 (2007).

#162929 - $15.00 USD Received 13 Feb 2012; revised 16 Mar 2012; accepted 16 Mar 2012; published 26 Mar 2012

12. W. Wasilewski and M. G. Raymer, "Pairwise entanglement and readout of atomic-ensemble and optical wave-packet modes in traveling-wave Raman interactions," Phys. Rev. A **73**, 063816 (2006).
13. D. Kielpinski, J. Corney, and H. Wiseman, "Quantum optical waveform conversion," Phys. Rev. Lett. **106**, 130501 (2011).
14. A. Eckstein, B. Brecht, and C. Silberhorn, "A quantum pulse gate based on spectrally engineered sum frequency generation," Opt. Express **19**, 13770–13778 (2011).
15. W. K. Wootters and W. H. Zurek, "A single quantum cannot be cloned," Nature (London) **299**, 802–803 (1982).
16. W. H. Louisell, A. Yariv, and A. E. Siegman, "Quantum fluctuations and noise in parametric processes I," Phys. Rev. **124**, 1646–1653 (1961).
17. J. P. Gordon, W. H. Louisell, and L. R. Walker, "Quantum fluctuations and noise in parametric processes II," Phys. Rev. **129**, 481–485 (1963).
18. J. Huang and P. Kumar, "Observation of quantum frequency conversion," Phys. Rev. Lett. **68**, 2153–2156 (1992).
19. A. P. Vandevender and P. G. Kwiat, "High efficiency single photon detection via frequency up-conversion," J. Mod. Opt. **51**, 1433–1445 (2004).
20. M. A. Albota and F. N. C. Wong, "Efficient single-photon counting at 1.55 μm by means of frequency upconversion," Opt. Lett. **29**, 1449–1451 (2004).
21. R. V. Roussev, C. Langrock, J. R. Kurz, and M. M. Fejer, "Periodically poled lithium niobate waveguide sum-frequency generator for efficient single-photon detection at communication wavelengths," Opt. Lett. **29**, 1518–1520 (2004).
22. Y. Ding and Z. Y. Ou, "Frequency downconversion for a quantum network," Opt. Lett. **35**, 2591–2593 (2010).
23. B. Brecht, A. Eckstein, A. Christ, H. Suche, and C. Silberhorn, "From quantum pulse gate to quantum pulse shaper–engineered frequency conversion in nonlinear optical waveguides," New J. Phys. **13**, 065029 (2011).
24. C. Clausen, I. Usmani, F. Bussières, N. Sangouard, M. Afzelius, H. de Riedmatten, and N. Gisin, "Quantum storage of photonic entanglement in a crystal," Nature (London) **469**, 508–511 (2011).
25. E. Saglamyurek, N. Sinclair, J. Jin, J. Slater, D. Oblak, F. Bussières, M. George, R. Ricken, W. Sohler, and W. Tittel, "Broadband waveguide quantum memory for entangled photons," Nature (London) **469**, 512–515 (2011).
26. C. J. McKinstrie, J. D. Harvey, S. Radic, and M. G. Raymer, "Translation of quantum states by four-wave mixing in fibers," Opt. Express **13**, 9131–9142 (2005).
27. K. Inoue, "Tunable and selective wavelength conversion using fiber four-wave mixing with two pump lights," IEEE Photon Technol. Lett. **6**, 1451–1453 (1994).
28. M. E. Marhic, Y. Park, F. S. Yang, and L. G. Kazovsky, "Widely tunable spectrum translation and wavelength exchange by four-wave mixing in optical fibers," Opt. Lett. **21**, 1906–1908 (1996).
29. K. Uesaka, K. K. Wong, M. E. Marhic, and L. G. Kazovsky, "Wavelength exchange in a highly nonlinear dispersion-shifted fiber: theory and experiments," IEEE J. Sel. Top. Quantum Electron. **8**, 560–568 (2002).
30. T. Tanemura, C. S. Goh, K. Kikuchi, and S. Y. Set, "Highly efficient arbitrary wavelength conversion within entire C-band based on nondegenerate fiber four-wave mixing," IEEE Photon. Technol. Lett. **16**, 551–553 (2004).
31. A. H. Gnauck, R. M. Jopson, C. J. McKinstrie, J. C. Centanni, and S. Radic, "Demonstration of low-noise frequency conversion by Bragg scattering in a fiber," Opt. Express **14**, 8989–8994 (2006).
32. D. Méchin, R. Provo, J. D. Harvey, and C. J. McKinstrie, "180-nm wavelength conversion based on Bragg scattering in an optical fiber," Opt. Express **14**, 8995–8999 (2006).
33. H. J. McGuinness, M. G. Raymer, C. J. McKinstrie, and S. Radic, "Wavelength translation across 210 nm in the visible using vector Bragg scattering in a birefringent photonic crystal fiber," IEEE Photon. Technol. Lett. **23**, 109–111 (2011).
34. H. J. McGuinness, M. G. Raymer, C. J. McKinstrie, and S. Radic, "Quantum frequency translation of single-photon states in a photonic crystal fiber," Phys. Rev. Lett. **105**, 093604 (2010).
35. C. J. McKinstrie, H. Kogelnik, R. M. Jopson, S. Radic, and A. V. Kanaev, "Four-wave mixing in fibers with random birefringence," Opt. Express **12**, 2033–2055 (2004).
36. C. J. McKinstrie, M. Yu, M. G. Raymer, and S. Radic, "Quantum noise properties of parametric processes," Opt. Express **13**, 4986–5012 (2005).
37. M. G. Raymer, S. J. van Enk, C. J. McKinstrie, and H. J. McGuinness, "Interference of two photons of different color," Opt. Commun. **283**, 747–752 (2010).
38. H. J. McGuinness, M. G. Raymer, and C. J. McKinstrie, "Theory of quantum frequency translation of light in optical fiber: application to interference of two photons of different color," Opt. Express **19**, 17876–17907 (2011).
39. K. Inoue, "Polarization effect on four-wave mixing efficiency in a single-mode fiber," IEEE J. Quantum Electron. **28**, 883–894 (1992).
40. M. E. Marhic, K. K. Y. Wong, and L. G. Kazovsky, "Fiber optical parametric amplifiers with linearly or circularly polarized waves," J. Opt. Soc. Am. B **20**, 2425–2433 (2003).
41. C. J. McKinstrie, H. Kogelnik, and L. Schenato, "Four-wave mixing in a rapidly-spun fiber," Opt. Express **14**, 8516–8534 (2006).
42. X. Li, P. L. Voss, J. Chen, K. F. Lee and P. Kumar, "Measurement of co- and cross-polarized Raman spectra in

#162929 - $15.00 USD Received 13 Feb 2012; revised 16 Mar 2012; accepted 16 Mar 2012; published 26 Mar 2012

silica fiber for small detunings," Opt. Express **13**, 2236–2244 (2005).
43. R. Loudon, *The Quantum Theory of Light*, 3rd. ed. (Oxford University Press, 2000).
44. C. K. Law, I. A. Walmsley, and J. H. Eberly, "Continuous frequency entanglement: effective finite Hilbert space and entropy control," Phys. Rev. Lett. **84**, 5304–5307 (2000).
45. C. J. McKinstrie, "Unitary and singular value decompositions of parametric processes in fibers," Opt. Commun. **282**, 583–593 (2009).
46. R. A. Horn and C. R. Johnson, *Matrix Analysis* (Cambridge University Press, 1990).
47. M. P. des Chênes, "Mémoire sur les séries et sur l'intégration complète d'une équation aux différences partielles linéaire du second ordre, à coefficients constants," Mémoires présentés à l'Institut des Sciences, Lettres et Arts, par divers savans, et lus dans ses assemblées. Sciences, mathématiques et physiques, 638–648 (1806).
48. W. P. Grice, A. B. U'Ren, and I. A. Walmsley, "Eliminating frequency and space-time correlations in multiphoton states," Phys. Rev. A **64**, 063815 (2001).
49. A. B. U'Ren, C. Silberhorn, K. Banaszek, I. A. Walmsley, R. Erdmann, W. P. Grice, and M. G. Raymer, "Generation of pure-state single-photon wavepackets by conditional preparation based on spontaneous parametric downconversion," Laser Phys. **15**, 146–161 (2005).
50. G. B. Whitham, *Linear and Nonlinear Waves* (Wiley, 1974), Chap. 2.
51. J. Goodman, *Introduction to Fourier Optics* (McGraw-Hill, 1968).
52. G. F. Simmons, *Differential Equations with Applications and Historical Notes*, 2nd. ed. (McGraw-Hill, 1991).
53. C. J. McKinstrie and D. S. Cargill, "Simultaneous frequency conversion, regeneration and reshaping of optical signals," Opt. Express **20**, 6881–6886 (2012).
54. F. G. Mehler, "Über die Entwicklung einer Funktion von beliebig vielen Variablen nach Laplaceshen Functionen höherer Ordnung," Journal für die reine und angewandte Mathematik, 161–176 (1866).
55. P. M. Morse and H. Feschbach, *Methods of Theoretical Physics* (McGraw-Hill, 1953), pp. 781 and 786.
56. E. Schmidt, "Zur Theorie der linearen und nichtlinearen Integralgleichungen," Mathematische Annalen **63**, 433–476 (1907).
57. B. L. Moiseiwitsch, *Integral Equations* (Dover, 2005).
58. C. J. McKinstrie and J. P. Gordon, "Field fluctuations produced by parametric processes in fibers," IEEE J. Sel. Top. Quantum Electron. **18**, 958–969 (2012).

1. Introduction

As the computational needs of the world keep increasing, quantum information (QI) processing is of increasing interest [1, 2]. A fundamental process in QI is Hong-Ou-Mandel interference (HOM), in which two photons interfere through a quantum optical effect [3]. Originally HOM interference was used to measure the delay between photons, but it has recently also been used in a scheme for quantum computation using linear optics [4, 5].

For quantum key distribution and continuous variable teleportation it has been shown that inseparable three-mode entanglement is useful [6]. This has been demonstrated in optical crystals using consecutive nonlinear optical interactions in resonance [6–9]. Recently it has been demonstrated, theoretically and experimentally, that three-color tripartite entanglement is possible in an optical parametric oscillator across a wide frequency range [10, 11].

A reliable and noise-free process for the translation (frequency conversion without conjugation) of a quantum-state from one frequency to another is required for QI to be able to send states from one quantum node to another [1, 2]. These states could be stored in quantum memories corresponding to wavelengths from 300–800 nm that need to be transmitted over a traditional optical link with the low-loss windows in the range 1300–1600 nm [12–14]. It is important to note that this process does not violate the no-cloning theorem since the original state is destroyed in the process [15]. Quantum frequency conversion (QFC) was first investigated using three-wave mixing (TWM) in optical crystals where a strong pump p mitigates the conversion from the signal s to the idler r, *i.e.* $\pi_{\rm s} \leftrightarrow \pi_{\rm p} + \pi_{\rm r}$ where π_j represents a photon at frequency ω_j, $j \in \{\rm p,r,s\}$. The theoretical ground-work for QFC using TWM was presented in [16, 17] and first demonstrated experimentally in [18]. This process has been used for higher-efficiency single-photon detection using frequency up-conversion [19–21] and also for quantum networks using frequency down-conversion [22]. It has been demonstrated theoretically that TWM allows reshaping of pulses (*i.e.* from a continuous-wave to a short pulse and vice versa) when

#162929 - $15.00 USD Received 13 Feb 2012; revised 16 Mar 2012; accepted 16 Mar 2012; published 26 Mar 2012

using spectral phase modulation and propagation [13] or using dispersion engineering [23]. This is an important result since the states emitted from current quantum memory units have a pulse width many times larger than what is desired for traditional optical communication links [13, 14, 24, 25].

QFC is also possible using non-degenerate four-wave mixing (FWM) in an optical-fiber [26]. It is in the form of Bragg scattering (BS), which is characterized by two strong pumps p and q that interact with two sidebands r and s such that $\pi_\mathrm{p}+\pi_\mathrm{s}\leftrightarrow\pi_\mathrm{q}+\pi_\mathrm{r}$. See Fig. 1 for the frequency locations of the four fields. This process has been used classically to allow FC (frequency conversion) over a wide frequency range [27–29]. The advantages of BS are that it is tunable [30], has low-noise transfer [31], and allows for very distant FC (more than 200 nm) [32, 33]. BS has also been used to FC single photons [34].

One advantage of QFC using four-wave mixing in optical fibers is that the emitted photon wavepacket has a transverse distribution that is already mode-matched to existing transmission fibers. Also it allows for a very broad bandwidth of conversion as well as coupling from the visible to the telecom band and inter-telcom band conversion [26]. The quantum-noise properties of parametric amplification were considered in [35, 36] and it has theoretically been shown that BS allows for noiseless QFC [26]. BS has also been shown theoretically to allow HOM-interference between photons of different colors [37, 38].

In this paper we describe the Green-function formalism for FC and the Schmidt decomposition in Section 2. The advantage of the Schmidt decomposition is that it allows for an easy interpretation of the results as it describes the natural modes of the process and the conversion between them. In Section 3 FC is solved in the perturbative regime, *i.e.* low energy-conversion efficiency. The low-efficiency regime allows simple analytic solutions, including the Schmidt decomposition, which provide baseline theoretical results to which to compare higher-efficiency results typically obtained numerically, where it is found that up to about 50 % efficiency the exact numerical results bear high similarity to the perturbative ones [38]. The walk-off (pump convection) between the pumps is ignored. In Section 4 convection of the pumps is included and the differences between the two models highlighted. In both cases the results are decomposed and the Schmidt coefficients (mode-conversion efficiencies) and the Schmidt modes (input and output modes) are related to physical parameters: the pump energy, pump width, fiber length and the dispersion-induced sideband walk-off. We find that re-shaping is indeed possible using BS, due to the presence of the two pumps. Furthermore this process does not require dispersion engineering or additional processing like what is required for TWM.

2. General formalism of FC

Frequency conversion using four-wave mixing (FWM) includes the two pumps p and q as well as the two sidebands r and s, and comes in two different flavors: near and far conversion, see Fig. 1. This process is governed by the coupled-mode equations (CMEs) [26, 38]

$$(\partial_z+\beta_\mathrm{r}\partial_t)A_\mathrm{r}=\mathrm{i}\,\gamma_\mathrm{pq}A_\mathrm{s}, \tag{1}$$

$$(\partial_z+\beta_\mathrm{s}\partial_t)A_\mathrm{s}=\mathrm{i}\,\gamma_\mathrm{pq}^*A_\mathrm{r}, \tag{2}$$

where ∂_z and ∂_t are partial derivatives with respect to z and t respectively, β_r and β_s are the group slownesses (inverse group speeds) of the idler and the signal respectively, while $A_\mathrm{r}(t,z)$ and $A_\mathrm{s}(t,z)$ are the corresponding sideband amplitudes. Finally, $\gamma_\mathrm{pq}=\gamma A_\mathrm{p}(t-\beta_\mathrm{s}z)A_\mathrm{q}^*(t-\beta_\mathrm{r}z)$ which is based on the reasonable assumption that pump p co-propagates with sideband s and pump q co-propagates with sideband r [38]. In the case where the four fields are co-polarized and furthermore when the pumps fulfill the normalization condition $\int|A_j(t)|^2\,\mathrm{d}t=1$, we write $\gamma=2\gamma_\mathrm{K}(E_\mathrm{p}E_\mathrm{q})^{1/2}$ where γ_K is the Kerr nonlinearity coefficient and E_j, $j\in\{\mathrm{p},\mathrm{q}\}$, are the

#162929 - $15.00 USD Received 13 Feb 2012; revised 16 Mar 2012; accepted 16 Mar 2012; published 26 Mar 2012

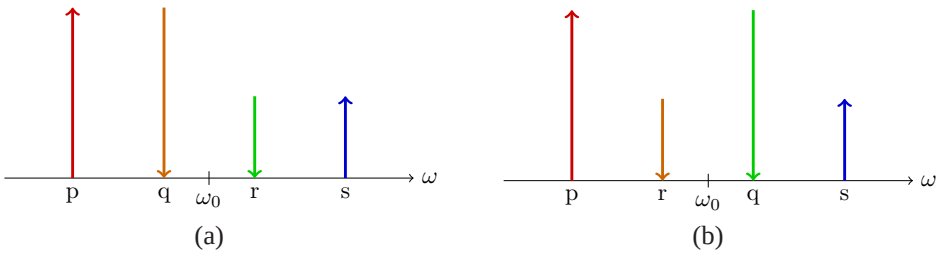

Fig. 1. (a) The placement in the frequency spectrum of the two pumps p and q along with the sidebands s and i for frequency conversion in the near-conversion regime. ω_0 is the zero-dispersion frequency. In this case the two pumps are closely spaced in frequency. (b) Illustration of frequency conversion in the far-conversion regime. Here the pumps are farther from each other. Arrows pointing up denote creation of photons and arrows pointing down destruction of photons.

pump energies. In the low-efficiency regime self-phase and cross-phase modulation are negligible. Intra-channel dispersion was also neglected which is a reasonable assumption for a recent experiment [34, 38] and a wide variety of related experiments. The case with different polarizations is considered in [35, 39–41]. The effect of spontaneous Raman scattering (SRS) is not modeled by Eqs. (1) and (2). The effect of SRS is minimized for very small or very large ($\gg 13\,\mathrm{THz}$) frequency shifts. Very large frequency shifts were demonstrated in [32, 33]. As shown in [42] SRS is weaker for cross-polarized signals than co-polarized signals, so utilizing vector BS might diminish the effect. In [34] SRS was minimized by having the pumps at longer wavelengths than the sidebands, which meant that SRS was observed but FC was still achievable.

Equations (1) and (2) also apply to quantum mechanical operators, where the classical fields A_j are replaced with the mode operators $\hat{a}_j$ [26, 34]. It is known that beam splitters do not add excess noise [43], and since FC by BS has mathematically equivalent input-output (IO) relations it does also not add excess noise [26]. The mode operators satisfy the boson commutation relations

$$\left[\hat{a}_i(t),\hat{a}_j(t')\right]=0 \quad \text{and} \quad \left[\hat{a}_i(t),\hat{a}_j^{\dagger}(t')\right]=\delta_{ij}\,\delta(t-t'), \tag{3}$$

with $i,j\in\{\mathrm{r},\mathrm{s}\}$, δ_{ij} is the Kronecker delta and $\delta(t-t')$ is the Dirac delta function. The CMEs are valid in the so-called parametric approximation, in which the pumps are treated as strong continuous fields, and for which quantum fluctuations are ignored. The weak sidebands, however, are treated quantum mechanically.

Using the Green-function formalism, it is possible to write the solution of the CMEs in the IO form [37, 38]

$$A_j(t,l)=\sum_k\int_{-\infty}^{\infty}G_{jk}(t,l;t',0)A_k(t',0)\,\mathrm{d}t'. \tag{4}$$

From this equation, the output of mode j at (t,l) is described by a function G_{jk} that represents the influence of the input-mode k at $(t',0)$. In our example with two sidebands $k\in\{\mathrm{r},\mathrm{s}\}$, Eq. (4) leads to

$$A_\mathrm{r}(t)=\int_{-\infty}^{\infty}G_{\mathrm{rr}}(t;t')A_\mathrm{r}(t')\,\mathrm{d}t'+\int_{-\infty}^{\infty}G_{\mathrm{rs}}(t;t')A_\mathrm{s}(t')\,\mathrm{d}t', \tag{5}$$

where the short notation $G_{jk}(t;t')=G_{jk}(t,l;t',0)$ has been introduced and with t and t' as output and input times respectively. Similarly, A_s is described by the shape of itself and sideband r at

#162929 - $15.00 USD Received 13 Feb 2012; revised 16 Mar 2012; accepted 16 Mar 2012; published 26 Mar 2012

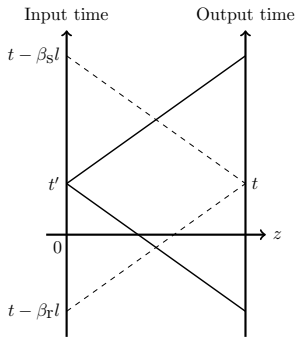

Fig. 2. A characteristic diagram for the generation of an idler from pulsed pumps for $\beta_r = -\beta_s$. The solid diagonal lines show the influence from the signal at the input point $(t',0)$ whereas the dashed lines show the domain that influences the output idler at (t,l) from the time-dependent pumps.

the input of the fiber. Physically this means that $G_{rr}(t;t')$ and $G_{ss}(t;t')$ describe the influence on the output at time t, from the input of the field itself at time t', see Fig. 2. In a similar way, the cross Green functions $G_{rs}(t;t')$ and $G_{sr}(t;t')$ concern the influence on one sideband at time t, from the other sideband at the input at time t'.

It is convenient to introduce the singular value (Schmidt) decomposition of the Green's functions since it allows us to split the Green function into products of functions that depend only on the input and output times at the cost of an infinite sum [44]. In general we write

$$G(t;t') = \sum_n v_n(t)\lambda_n^{1/2}u_n(t'), \tag{6}$$

where the functions u_n and v_n are the Schmidt modes normalized with respect to the integral of the absolute value squared. The normalized functions as well as the Schmidt coefficients $\lambda_n^{1/2}$ are found from the integral eigenvalue equations

$$\int_{-\infty}^{\infty} K_1(t,t')v_n(t')\,\mathrm{d}t' = \lambda_n v_n(t), \tag{7}$$

$$\int_{-\infty}^{\infty} K_2(t,t')u_n(t')\,\mathrm{d}t' = \lambda_n u_n(t), \tag{8}$$

with the kernels $K_1(t,t') \equiv \int G(t;t_2)G^*(t';t_2)\,\mathrm{d}t_2$ and $K_2(t,t') \equiv \int G(t_1;t)G^*(t_1;t')\,\mathrm{d}t_1$. We remind the reader that the first argument of the Green function corresponds to the output and the second argument to the input. The physical interpretation of the Schmidt decomposition is thus that it takes the input mode u_n and converts it to the output mode v_n with the probability λ_n [37, 38]. In matrix notation, the preceding decomposition can be rewritten simply as [45] $G = VDU^\dagger$, with V and U being (different) unitary matrices and D a diagonal matrix containing the non-negative square roots of the eigenvalues of the non-negative matrix $GG^\dagger$ (which are equal to the eigenvalues of $G^\dagger G$). Likewise V contains in its columns the eigenvectors of $GG^\dagger$ and the columns of U the eigenvectors of $G^\dagger G$ [46].

The properties of FC by BS is governed by the forward transformation matrix

$$\begin{bmatrix} G_{rr} & G_{rs} \\ G_{sr} & G_{ss} \end{bmatrix}, \tag{9}$$

#162929 - $15.00 USD Received 13 Feb 2012; revised 16 Mar 2012; accepted 16 Mar 2012; published 26 Mar 2012

where each of the Green functions has an expansion of the form (6). The fact that QFC is a unitary process, in the sense that quantum probability is conserved, leads to two important consequences. First the backward transformation matrix is simply the Hermitian conjugate of the forward transformation matrix [37], which is not true for parametric amplification. Second, the Schmidt decompositions of the constituent matrices are related through [12, 38]

$$\begin{bmatrix} G_{\mathrm{rr}} & G_{\mathrm{rs}} \\ G_{\mathrm{sr}} & G_{\mathrm{ss}} \end{bmatrix} = \sum_n \begin{bmatrix} v_{\mathrm{r},n}(t)\tau_n u^*_{\mathrm{r},n}(t') & v_{\mathrm{r},n}(t)\rho_n u^*_{\mathrm{s},n}(t') \\ -v_{\mathrm{s},n}(t)\rho^*_n u^*_{\mathrm{r},n}(t') & v_{\mathrm{s},n}(t)\tau^*_n u^*_{\mathrm{s},n}(t') \end{bmatrix}. \tag{10}$$

where all four Green functions depend on the output time t and the input time t'. Furthermore $|\tau|^2_n$ is the transmission (nonconversion) probability and $|\rho|^2_n$ is the frequency conversion probability. We have the requirement $|\rho_n|^2 + |\tau_n|^2 = 1$ due to photon number conservation. The symmetry of this expansion is clear. Conversion from one sideband is described by the same input modes and, similarly, conversion to a sideband is described by identical output modes. In the case with only one non-zero Schmidt coefficient we obtain mode-filtering, since a lot of modes may be sent in, but only one is converted. Similarly for the case of many non-zero Schmidt coefficients we have mode non-filtering in the sense that the output is the sum of many inputs [38].

2.1. The frequency and time domains

Some aspects of the FC process are easier to model in the time domain, and others are easier to model in the frequency domain. Thus this section considers the relations between the two domains. The following analysis is based on the symmetric Fourier-transform

$$\mathscr{F}\{A(t)\} = (2\pi)^{-1/2} \int_{-\infty}^{\infty} A(t) \exp(\mathrm{i}\omega t)\, \mathrm{d}t, \tag{11}$$

$$\mathscr{F}^{-1}\{A(\omega)\} = (2\pi)^{-1/2} \int_{-\infty}^{\infty} A(\omega) \exp(-\mathrm{i}\omega t)\, \mathrm{d}\omega. \tag{12}$$

The Fourier-transform of functions of two variables is defined in a similar way. Considering the input-output (IO) equation, Eq. (5), ignoring the self-band interactions, and taking the Fourier-transform with respect to ω_{r} yields

$$A_{\mathrm{r}}(\omega_{\mathrm{r}}) = \int_{-\infty}^{\infty} G_{\mathrm{rs}}(\omega_{\mathrm{r}}; t') A_{\mathrm{s}}(t')\, \mathrm{d}t'. \tag{13}$$

A product in the time-domain is the inverse Fourier-transform of a convolution in the frequency-domain, so

$$A_{\mathrm{r}}(\omega_{\mathrm{r}}) = (2\pi)^{-1} \iint_{-\infty}^{\infty} \mathrm{d}t' \mathrm{d}\omega_{\mathrm{s}} \int_{-\infty}^{\infty} \mathrm{d}\omega G_{\mathrm{rs}}(\omega_{\mathrm{r}}; \omega_{\mathrm{s}} - \omega) A_{\mathrm{s}}(\omega) \exp(-\mathrm{i}\omega_{\mathrm{s}} t') \tag{14}$$

We remind the reader of the relation, $\int_{-\infty}^{\infty} \exp(\pm \mathrm{i}\omega t)\, \mathrm{d}t = 2\pi\, \delta(\omega)$, from which the IO relation in the frequency-domain is obtained

$$A_{\mathrm{r}}(\omega_{\mathrm{r}}) = \int_{-\infty}^{\infty} G_{\mathrm{rs}}(\omega_{\mathrm{r}}; -\omega_{\mathrm{s}}) A_{\mathrm{s}}(\omega_{\mathrm{s}})\, \mathrm{d}\omega_{\mathrm{s}}. \tag{15}$$

Similarly, the signal Green function in the frequency domain is given as

$$A_{\mathrm{s}}(\omega_{\mathrm{s}}) = \int_{-\infty}^{\infty} G_{\mathrm{sr}}(\omega_{\mathrm{s}}; -\omega_{\mathrm{r}}) A_{\mathrm{r}}(\omega_{\mathrm{r}})\, \mathrm{d}\omega_{\mathrm{r}}. \tag{16}$$

#162929 - $15.00 USD Received 13 Feb 2012; revised 16 Mar 2012; accepted 16 Mar 2012; published 26 Mar 2012

The Fourier transform of the Green function is given as

$$G_{\mathrm{rs}}(\omega_{\mathrm{r}};-\omega_{\mathrm{s}}) = (2\pi)^{-1}\iint_{-\infty}^{\infty} G_{\mathrm{rs}}(t;t')\exp(\mathrm{i}\omega_{\mathrm{r}}t - \mathrm{i}\omega_{\mathrm{s}}t')\,\mathrm{d}t\mathrm{d}t', \tag{17}$$

$$G_{\mathrm{rs}}(t;t') = (2\pi)^{-1}\iint_{-\infty}^{\infty} G_{\mathrm{rs}}(\omega_{\mathrm{r}};-\omega_{\mathrm{s}})\exp(-\mathrm{i}\omega_{\mathrm{r}}t + \mathrm{i}\omega_{\mathrm{s}}t')\,\mathrm{d}\omega_{\mathrm{r}}\mathrm{d}\omega_{\mathrm{s}}. \tag{18}$$

Another interesting aspect is the Fourier-transform of the Schmidt-decomposed Green functions. Suppose that the time-domain Green function has the Schmidt-decomposition

$$G_{\mathrm{rs}}(t;t') = \sum_{n=0}^{\infty} \lambda_n^{1/2} v_n(t) u_n^*(t'), \tag{19}$$

and when using Eqs. (17) and (19) gives

$$\begin{aligned} G_{\mathrm{rs}}(\omega_{\mathrm{r}};-\omega_{\mathrm{s}}) = \sum_{n=0}^{\infty} \lambda_n^{1/2} &\int_{-\infty}^{\infty} v_n(t)\exp(\mathrm{i}\omega_{\mathrm{r}}t)(2\pi)^{-1/2}\,\mathrm{d}t \\ &\times \int_{-\infty}^{\infty} \left[u_n(t')\exp(\mathrm{i}\omega_{\mathrm{s}}t_{\mathrm{s}})\right]^* (2\pi)^{-1/2}\,\mathrm{d}t', \end{aligned} \tag{20}$$

where we have exchanged the order of the sum and the integral which is allowed since the sum by definition is convergent. This form shows that the Fourier transform of the Schmidt decomposition of the Green function involves only the Fourier-transform of the individual input and output modes

$$G_{\mathrm{rs}}(\omega_{\mathrm{r}};-\omega_{\mathrm{s}}) = \sum_{n=0}^{\infty} \lambda_n^{1/2} v_n(\omega_{\mathrm{r}}) u_n^*(\omega_{\mathrm{s}}). \tag{21}$$

We also note from Parseval's identity that if the eigenfunctions are normalized in the time-domain they are also normalized in the frequency-domain [47]. The Schmidt coefficients, $\lambda_n^{1/2}$ are naturally identical in the two domains. In the special case where $u_n(t)$ are real the relation $u_n^*(\omega) = u(-\omega)$ holds. A similar result exists when going from the frequency-domain to the time-domain. That is the Fourier transform of the Green function is the sum of products of the Fourier transform of the Schmidt modes. This is an important result that is used extensively through the remainder of this paper.

3. Stationary pumps

To gain physical insight we start by solving the FC problem in the low-conversion regime while assuming that the pumps do not convect relative to one another in the moving frame propagating at the average group slowness of the sidebands. This is a simplified model of FWM, since in most cases the pumps walk-off with respect to each other. However it is representative of TWM, because one pump is always stationary. One may simply choose the frame of reference to propagate with the pump. First we derive the equations in the frequency-domain, since this is the standard approach and afterwards we present an alternative derivation.

By Fourier transforming Eqs. (1) and (2) with respect to t and t' one find that

$$\partial_z A_{\mathrm{r}}(\omega_{\mathrm{r}},z) = \mathrm{i}\beta_{\mathrm{r}}(\omega_{\mathrm{r}})A_{\mathrm{r}}(\omega_{\mathrm{r}},z) + \mathrm{i}\,(2\pi)^{-1/2}\int_{\infty}^{\infty}\gamma_{\mathrm{pq}}(\omega_{\mathrm{r}}-\omega_{\mathrm{s}},z)A_{\mathrm{s}}(\omega_{\mathrm{s}})\,\mathrm{d}\omega_{\mathrm{s}}, \tag{22}$$

$$\partial_z A_{\mathrm{s}}(\omega_{\mathrm{s}},z) = \mathrm{i}\beta_{\mathrm{s}}(\omega_{\mathrm{s}})A_{\mathrm{s}}(\omega_{\mathrm{s}},z) + \mathrm{i}\,(2\pi)^{-1/2}\int_{\infty}^{\infty}\gamma^*_{\mathrm{pq}}(\omega_{\mathrm{s}}-\omega_{\mathrm{r}},z)A_{\mathrm{r}}(\omega_{\mathrm{r}})\,\mathrm{d}\omega_{\mathrm{r}}. \tag{23}$$

Introducing the transformed field $A_j(\omega_j,z) = B_j(\omega_j,z)\exp[\mathrm{i}\beta_j(\omega_j)z]$ simplifies the analysis. Furthermore it is assumed that $\beta_j(\omega_j) = \beta_j^{(1)}\omega_j$, thus neglecting group velocity dispersion and

#162929 - $15.00 USD Received 13 Feb 2012; revised 16 Mar 2012; accepted 16 Mar 2012; published 26 Mar 2012

higher-order effects, *i.e.* $\beta_j^{(3)}, \beta_j^{(4)}, \ldots$, which is reasonable for a sufficiently short piece of fiber and a narrow pulse in the frequency domain. Throughout the remainder of this paper the simpler notation $\beta_j^{(1)} = \beta_j$ is used for the group slowness. These assumptions lead to the approximate solutions [38]

$$B_{\mathrm{r}}(\omega_{\mathrm{r}}, l) \approx \mathrm{i}(2\pi)^{-1/2} \int_0^l \int_{-\infty}^{\infty} \gamma_{\mathrm{pq}}(\omega_{\mathrm{r}} - \omega_{\mathrm{s}}, z) \exp(\mathrm{i}z\omega_{\mathrm{s}}\beta_{\mathrm{s}}) \times \exp(-\mathrm{i}z\omega_{\mathrm{r}}\beta_{\mathrm{r}}) B_{\mathrm{s}}(\omega_{\mathrm{s}}, 0)\, \mathrm{d}\omega_{\mathrm{s}}\, \mathrm{d}z, \tag{24}$$

where l is the fiber length. A similar expression exists for the signal field. Using Eqs. (15) and (16), and inserting $B_j = A_j \exp[-\mathrm{i}\beta_j(\omega_j)z]$, one finds the Green functions

$$G_{\mathrm{rs}}(\omega_{\mathrm{r}}; -\omega_{\mathrm{s}}) = \mathrm{i}(2\pi)^{-1/2} \int_0^l \gamma_{\mathrm{pq}}(\omega_{\mathrm{r}} - \omega_{\mathrm{s}}, z) \exp\left[\mathrm{i}\beta_{\mathrm{r}}(l-z)\omega_{\mathrm{r}} + \mathrm{i}\beta_{\mathrm{s}} z \omega_{\mathrm{s}}\right] \mathrm{d}z, \tag{25}$$

$$G_{\mathrm{sr}}(\omega_{\mathrm{s}}; -\omega_{\mathrm{r}}) = \mathrm{i}(2\pi)^{-1/2} \int_0^l \gamma^*_{\mathrm{pq}}(\omega_{\mathrm{s}} - \omega_{\mathrm{r}}, z) \exp\left[\mathrm{i}\beta_{\mathrm{s}}(l-z)\omega_{\mathrm{s}} + \mathrm{i}\beta_{\mathrm{r}} z \omega_{\mathrm{r}}\right] \mathrm{d}z. \tag{26}$$

3.1. Standard analysis

The standard way to find the Green function is to consider a specific pump-shape and to carry out the z-integral in the frequency-domain [48]. A typical pump-shape choice is two identical Gaussian pumps. It is assumed that the pumps do not convect, thus we write them in the form

$$A_{\mathrm{p}}(t) = A_{\mathrm{q}}(t) = (\pi\tau_0^2)^{-1/4} \exp[-t^2/(2\tau_0^2)], \tag{27}$$

where τ_0 is the root-mean-square width and where the pump-shapes are normalized. The Fourier transform of $\gamma_{\mathrm{pq}}(t)$ is

$$\gamma_{\mathrm{pq}}(\omega) = \gamma(2\pi)^{-1/2} \exp\left(-\sigma^2\omega^2/2\right), \tag{28}$$

with $\sigma = \tau_0/\sqrt{2}$. The factor $\gamma(2\pi)^{-1}$ is denoted γ_0 and includes the $(2\pi)^{-1/2}$ in front of the Green function. Inserting this in the Green function and integrating with respect to z leads to

$$G_{\mathrm{rs}}(\omega_{\mathrm{r}}; -\omega_{\mathrm{s}}) = \mathrm{i}\gamma_0 l \exp\left[\mathrm{i}\beta_{\mathrm{r}}\omega_{\mathrm{r}} l - \mathrm{i}l\delta_0/2 - \sigma^2(\omega_{\mathrm{r}} - \omega_{\mathrm{s}})^2/2\right] \mathrm{sinc}\left[l\delta_0/2\right], \tag{29}$$

with the walk-off parameter defined as $\delta_0 = \beta_{\mathrm{r}}\omega_{\mathrm{r}} - \beta_{\mathrm{s}}\omega_{\mathrm{s}}$. The next step is to approximate the sinc with a Gaussian, $\mathrm{sinc}(x) \approx \exp(-\xi x^2/2)$ with $\xi \approx 0.3858$. This value is chosen so that the sinc and the Gaussian have the same full-width-at-half-maximum (FWHM) [48]. All in all our Green function attains the form

$$G_{\mathrm{rs}}(\omega_{\mathrm{r}}; -\omega_{\mathrm{s}}) = \mathrm{i}\gamma_0 l \exp\left[\mathrm{i}l(\beta_{\mathrm{r}}\omega_{\mathrm{r}} + \beta_{\mathrm{s}}\omega_{\mathrm{s}})/2 - \sigma^2(\omega_{\mathrm{r}} - \omega_{\mathrm{s}})^2/2 - (\alpha_{\mathrm{r}}\omega_{\mathrm{r}} - \alpha_{\mathrm{s}}\omega_{\mathrm{s}})^2/2\right], \tag{30}$$

with $\alpha_j = \xi^{1/2}\beta_j l/2$. To discuss whether the Green function is separable in its two frequencies the Schmidt decomposition is introduced in Eq. (108) of the Appendix. Since λ_n is real by definition we cast the Schmidt decomposition of the Green function under the Gaussian approximation in the following form:

$$G_{\mathrm{rs}}(\omega_{\mathrm{r}}; -\omega_{\mathrm{s}}) = \mathrm{i} \sum_{n=0}^{\infty} \exp(\mathrm{i}l\beta_{\mathrm{r}}\omega_{\mathrm{r}}/2 + \mathrm{i}l\beta_{\mathrm{s}}\omega_{\mathrm{s}}/2) \lambda_n^{1/2} \phi_n(\tau_{\mathrm{r}}\omega_{\mathrm{r}}) \phi_n^*(\tau_{\mathrm{s}}\omega_{\mathrm{s}}), \tag{31}$$

where ϕ_n is the nth orthonormal Hermite polynomial

$$\phi_n(ax) = a^{1/2} H_n(ax) \exp[-(ax)^2/2]/[\pi^{1/4}(n!2^n)^{1/2}], \tag{32}$$

#162929 - $15.00 USD Received 13 Feb 2012; revised 16 Mar 2012; accepted 16 Mar 2012; published 26 Mar 2012

and where H_n is the Hermite polynomial of order n. The square of the Schmidt coefficient (the dilation factor) is in the form

$$\lambda_n = \frac{\pi(\gamma_0 l)^2}{\tau_\mathrm{r}\tau_\mathrm{s}}(1-\mu^2)\mu^{2n}. \tag{33}$$

The dimensionless separability parameter is given as

$$\mu = \frac{\left[\left(\sigma^2+\alpha_\mathrm{r}^2\right)\left(\sigma^2+\alpha_\mathrm{s}^2\right)\right]^{1/2}-\sigma\alpha_\mathrm{rs}}{\sigma^2+\alpha_\mathrm{r}\alpha_\mathrm{s}}, \tag{34}$$

where it is assumed without loss of generality that $\alpha_\mathrm{rs}=\alpha_\mathrm{r}-\alpha_\mathrm{s}$ is positive. The characteristic timescales are

$$\tau_\mathrm{r} = (\sigma|\alpha_\mathrm{r}-\alpha_\mathrm{s}|)^{1/2}\left(\frac{\sigma^2+\alpha_\mathrm{r}^2}{\sigma^2+\alpha_\mathrm{s}^2}\right)^{1/4}, \tag{35}$$

$$\tau_\mathrm{s} = (\sigma|\alpha_\mathrm{r}-\alpha_\mathrm{s}|)^{1/2}\left(\frac{\sigma^2+\alpha_\mathrm{s}^2}{\sigma^2+\alpha_\mathrm{r}^2}\right)^{1/4}. \tag{36}$$

Formula (33) for the Schmidt coefficient is simplified by the identity

$$\frac{\pi(1-\mu^2)}{\tau_\mathrm{r}\tau_\mathrm{s}} = \frac{2\pi}{[(\sigma^2+\alpha_\mathrm{r}^2)(\sigma^2+\alpha_\mathrm{s}^2)]^{1/2}+\sigma\alpha_\mathrm{rs}}, \tag{37}$$

which follows from Eqs. (34)–(36).

For many applications one is interested in separating the Green functions into functions depending on only one of the frequencies, as frequency entanglement is undesired for some quantum optical interference experiments [48, 49]. Separability has been studied extensively for photon-pair generation using three-wave mixing [48, 49], but not for FC. To achieve separability it is required that $\mu=0$ and, with the aforementioned assumption that $\alpha_\mathrm{rs}>0$, this leads to the separability requirement $\alpha_\mathrm{r}\alpha_\mathrm{s}=-\sigma^2$. In the co-propagating case (where the group slownesses of the sidebands have the same sign) it is not possible to obtain separability since σ is real, whereas in the counter-propagating case (with different signs of the inverse group velocities) it is possible to obtain separability for one specific length of the fiber. For $\mu=0$, this leads to considerably simpler parameters

$$\lambda_0 = \frac{\pi\gamma_0^2 l^2}{(\alpha_\mathrm{r}\alpha_\mathrm{s})^{1/2}\alpha_\mathrm{rs}}, \tag{38}$$

$$\tau_\mathrm{r} = (\sigma^2+\alpha_\mathrm{r}^2)^{1/2}, \tag{39}$$

$$\tau_\mathrm{s} = (\sigma^2+\alpha_\mathrm{s}^2)^{1/2}, \tag{40}$$

where λ_0 is the only non-zero squared Schmidt coefficient. Notice that this Schmidt coefficient is indeed independent of the fiber length.

It is instructive to cast Eq. (31) in a slightly different way:

$$G_\mathrm{rs}(\omega_\mathrm{r};-\omega_\mathrm{s}) = \mathrm{i}\sum_{n=0}^{\infty}\lambda_n^{1/2}v_n(\omega_\mathrm{r})u_n^*(\omega_\mathrm{s}), \tag{41}$$

with $v_n(\omega_\mathrm{r})=\phi_n(\tau_\mathrm{r}\omega_\mathrm{r})\exp(\mathrm{i}l\beta_\mathrm{r}\omega_\mathrm{r}/2)$ and $u_n(\omega_\mathrm{s})=\phi_n(\tau_\mathrm{s}\omega_\mathrm{s})\exp(-\mathrm{i}l\beta_\mathrm{s}\omega_\mathrm{s}/2)$. Since ω_r and ω_s correspond to the output and input frequencies respectively, we notice that τ_r and τ_s are characteristic time scales.

#162929 - $15.00 USD Received 13 Feb 2012; revised 16 Mar 2012; accepted 16 Mar 2012; published 26 Mar 2012

The time-domain Green function is found by Fourier transforming Eq. (30), see Appendix A for the details. The result is

$$G_{\rm rs}(t;t') = \frac{{\rm i}\gamma}{\pi\sigma\xi^{1/2}|\beta_{\rm rs}|}\exp\left[-\frac{(\sigma^2+\alpha_{\rm s}^2)\bar{t}^2 - 2(\sigma^2+\alpha_{\rm r}\alpha_{\rm s})\bar{t}\bar{t}' + (\sigma^2+\alpha_{\rm r}^2)(\bar{t}')^2}{2(\sigma\alpha_{\rm rs})^2}\right], \quad (42)$$

where the retarded (or advanced) times are $\bar{t} = t - \beta_{\rm r} l/2$ and $\bar{t}' = t' + \beta_{\rm s} l/2$.

According to the inverse of Eq. (21) the Fourier transform of the Schmidt decomposition is simply the Fourier transform of the individual Schmidt modes and since $\mathscr{F}^{-1}\left\{f(a\omega){\rm e}^{{\rm i}b\omega}\right\} = f[(t-b)/a]/|a|$, Eq. (41) becomes

$$G_{\rm rs}(t;t') = {\rm i}\sum_{n=0}^{\infty}\lambda_n^{1/2}\phi_n\left(\frac{t-\beta_{\rm r} l/2}{\tau_{\rm r}}\right)\phi_n^*\left(\frac{t'+\beta_{\rm s} l/2}{\tau_{\rm s}}\right), \quad (43)$$

where the Schmidt modes remain normalized and the square of the Schmidt coefficients are given in Eq. (33). This is the same decomposition we get by using Eqs. (104)–(107) to decompose Eq. (42), thus confirming the results in Eqs. (19) and (21). For the case in which $\beta_{\rm r} = -\beta_{\rm s}$ the input and output modes are shifted in phase by the factor $l\beta_j\omega_j/2$ corresponding to an interaction at the middle of the fiber which maximizes the interaction between the four fields [38].

3.2. Alternative analysis

The standard analysis in the frequency domain is based on two reasonable, but nonetheless restricting assumptions, *i.e.* similar Gaussian pumps and the approximation of the sinc-function with a Gaussian. We now present an alternative analysis that enables deriving the Green functions in the time-domain in the general case by interchanging the order of the frequency and length integrals. Finally we also present a simpler and more physical derivation.

Considering the Fourier transform of Eq. (25) (for brevity we only show a detailed derivation of $G_{\rm rs}$), which is

$$\begin{aligned} G_{\rm rs}(t;t') = {\rm i}(2\pi)^{-3/2}\int_0^l\iint_{-\infty}^{\infty}&\gamma_{\rm pq}(\omega_{\rm r}-\omega_{\rm s},z) \\ &\times\exp\left[-{\rm i}(t-\beta_{\rm r} l+\beta_{\rm r} z)\omega_{\rm r} + {\rm i}(t'+\beta_{\rm s} z)\omega_{\rm s}\right]{\rm d}\omega_{\rm r}{\rm d}\omega_{\rm s}{\rm d}z. \end{aligned} \quad (44)$$

Using the substitution $\omega_{\rm r}' = \omega_{\rm r} - \omega_{\rm s}$ and the Fourier transform property $\mathscr{F}^{-1}\left\{f(\omega){\rm e}^{a{\rm i}\omega}\right\} = f(t-a)$ leads to

$$G_{\rm rs}(t;t') = {\rm i}(2\pi)^{-1/2}\int_0^l\int_{-\infty}^{\infty}\gamma_{\rm pq}(t-\beta_{\rm r} l+\beta_{\rm r} z,z)\exp\left[{\rm i}\omega_{\rm s}(t'+\beta_{\rm s} z - t + \beta_{\rm r} l - \beta_{\rm r} z)\right]{\rm d}\omega_{\rm s}{\rm d}z. \quad (45)$$

Carrying out the second frequency integral gives a delta function in z, thus we find

$$G_{\rm rs}(t;t') = {\rm i}/|\beta_{\rm rs}|\,\gamma_{\rm pq}\left(\frac{\beta_{\rm r} t' - \beta_{\rm s}[t-\beta_{\rm r} l]}{\beta_{\rm rs}}, \frac{t'-t+\beta_{\rm r} l}{\beta_{\rm rs}}\right){\rm H}(t'+\beta_{\rm r} L - t)\,{\rm H}(t-t'-\beta_{\rm s} L), \quad (46)$$

where H is the Heaviside step-function, which ensures causality. This result is valid for arbitrary pump shapes, and it does not approximate the way the system responds [beyond the perturbation theory used to derive Eq. (25)]. The argument of $\gamma_{\rm pq}$ is a complicated function of t and t', but in the following section we present a simple physical derivation of it.

#162929 - $15.00 USD Received 13 Feb 2012; revised 16 Mar 2012; accepted 16 Mar 2012; published 26 Mar 2012

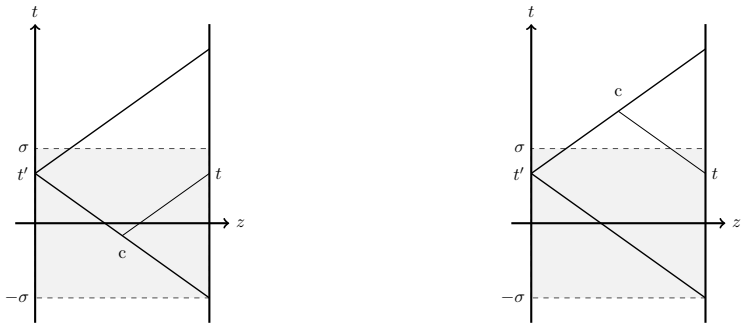

Fig. 3. Characteristic diagrams for (a) idler generation from a pulsed signal and (b) generation of a signal from a pulsed idler. The gray area shows the area of the high pump power region. The upward and downward diagonal lines are the characteristics of the idler and the signal respectively. The output idler (signal) at time t is generated by a collision with the signal (idler) occurring at the point c.

3.2.1. Time-domain collision analysis

Due to the simplicity of the Green function in the time-domain, Eq. (46), we find the Green functions directly, in the time domain, by using the method of characteristics [50]. In the low-conversion regime, the presence of the idler has little effect on the signal. Hence, a signal impulse that enters the fiber at time t' remains an impulse as it convects through the fiber. The part of the idler that exits the fiber at time t was generated by a collision of the idler pulse with the signal at the point (t_c, z_c), where $t' + \beta_s z_c = t - \beta_r(l - z_c)$. Such a collision is illustrated in Fig. 3a. The collision distance and time are

$$z_c = [t' - (t - \beta_r l)]/\beta_{rs}, \;\; t_c = [\beta_r t' - \beta_s(t - \beta_r l)]/\beta_{rs}, \tag{47}$$

respectively. After the collision, the idler convects with constant amplitude. By integrating Eq. (1) across the collision region, which is infinitesimally thin, one finds that the cross Green function is given approximately by

$$G_{rs}(t;t') \approx [\mathrm{i}\,\gamma_{pq}(z_c,t_c)/|\beta_{rs}|]\,\mathrm{H}(t' + \beta_r l - t)\,\mathrm{H}(t - t' - \beta_s l). \tag{48}$$

For signal generation by a pulsed idler, the collision distance and time are

$$z_c = [(t - \beta_s l) - t']/\beta_{rs}, \;\; t_c = [\beta_r(t - \beta_s l) - \beta_s t')]/\beta_{rs}, \tag{49}$$

respectively, see Fig. 3b. By repeating the collision analysis described above, one obtains the cross Green function

$$G_{sr}(t,t') \approx [\mathrm{i}\,\gamma^*_{pq}(z_c,t_c)/|\beta_{rs}|]\,\mathrm{H}(t' + \beta_r l - t)\,\mathrm{H}(t - t' - \beta_s l). \tag{50}$$

3.3. Comparing the time-domain and the frequency-domain results

The Green functions were found directly using the collision analysis, *cf.* Eq. (48). Notice that the collision time may be evaluated from

$$\beta_r t' - \beta_s(t - \beta_r l) = \beta_r(t' + \beta_s l/2) - \beta_s(t - \beta_r l/2) = \beta_r \overline{t'} - \beta_s \overline{t}, \tag{51}$$

#162929 - $15.00 USD Received 13 Feb 2012; revised 16 Mar 2012; accepted 16 Mar 2012; published 26 Mar 2012

where $\bar{t}_j$ are the same retarded times as used in Eq. (42). Second, notice that

$$\mathrm{H}(t-t'-\beta_\mathrm{s}l)\,\mathrm{H}(t'+\beta_\mathrm{r}l-t)=\mathrm{rect}[(t-t_\mathrm{a})/(\beta_\mathrm{rs}l)]=\mathrm{rect}[(\bar{t}-\bar{t}')/(\beta_\mathrm{rs}l)], \tag{52}$$

where the average time is $t_\mathrm{a}=t'+(\beta_\mathrm{r}+\beta_\mathrm{s})l/2$ and the rectangle function [51] is

$$\mathrm{rect}(x)=\begin{cases}1, & \text{if } |x|<1/2;\\ 1/2, & \text{if } x=\pm 1/2;\\ 0, & \text{otherwise.}\end{cases} \tag{53}$$

Thus, the Green function in Eq. (48) likewise only depends on the retarded times. The coupling function is defined as $\gamma_\mathrm{pq}(t)=\gamma A_\mathrm{p}(t)A_\mathrm{q}^*(t)$ where both pump shapes are normalized. To compare the Green functions in Eqs. (42) and (48) we pick

$$A_\mathrm{p}(t)A_\mathrm{q}^*(t)=\exp[-t^2/(2\sigma^2)]/(2\pi\sigma^2)^{1/2}. \tag{54}$$

In other words the Green function is of the form

$$G(t;t')=\frac{\mathrm{i}\gamma}{(2\pi)^{1/2}\sigma|\beta_\mathrm{rs}|}\exp\left[-\frac{(\beta_\mathrm{r}\bar{t}'-\beta_\mathrm{s}\bar{t})^2}{2(\beta_\mathrm{rs}\sigma)^2}\right]\mathrm{rect}\left(\frac{\bar{t}-\bar{t}'}{\beta_\mathrm{rs}l}\right). \tag{55}$$

To compare this result with the frequency-domain result that was derived using the sinc approximation, Eq. (42), the rectangular function is approximated with the Gaussian

$$h\exp\left[-\frac{(\bar{t}-\bar{t}')^2}{2w(\beta_\mathrm{rs}l/2)^2}\right], \tag{56}$$

where h and w are fitting parameters that will be determined later. For reference, $h=1$ produces the correct peak height, whereas $h=[2/(\pi w)]^{1/2}\approx 1.28$ produces the correct area. Aggregating these results the Green function is approximated by

$$G_\mathrm{rs}(t;t')\approx\frac{\mathrm{i}\gamma h}{(2\pi)^{1/2}\sigma|\beta_\mathrm{rs}|}\exp\left[-\frac{(\sigma^2+\alpha_\mathrm{s}^2)\bar{t}^2-2(\sigma^2+\alpha_\mathrm{r}\alpha_\mathrm{s})\bar{t}\bar{t}'+(\sigma^2+\alpha_\mathrm{r}^2)^2(\bar{t}')^2}{2(\sigma\alpha_\mathrm{rs})^2}\right], \tag{57}$$

where $\alpha_j=w^{1/2}\beta_j l/2$. Comparing Eqs. (42) and (57) they have the same general shape and we conclude that $w=\xi$ and $h=[2/(\pi w)]^{1/2}\approx 1.28$, which gives the same integral over the Gaussian and the rectangle function in the time domain. This shows that the effect of approximating the sinc with a Gaussian in the frequency-domain is equivalent to replacing the sharp boundaries from the rectangular function in the frequency-domain with a gradual effective boundary from the Gaussian. Physically this means that the Green function will allow effects from the input on the output from input and output times that are not allowed due to causality. Another issue is that in the limit of long fibers the rectangular function is unity for almost all times, so one has to pick $h=1$ to get the best results.

Since Eq. (57) is of the canonical form for the Schmidt decomposition of a Gaussian, see Eq. (104) in Appendix A, we notice that the square of the lowest-order Schmidt coefficient and time scales (μ_j is used instead of τ_j here not to confuse it with the pump-width) are in the form

$$\lambda_0=\frac{(\gamma h l)^2 w}{4[(\alpha_\mathrm{r}^2+\sigma^2)^{1/2}(\alpha_\mathrm{s}^2+\sigma^2)^{1/2}+\alpha_\mathrm{rs}\sigma]}, \tag{58}$$

$$\mu_\mathrm{r}=\frac{1}{(\alpha_\mathrm{rs}\sigma)^{1/2}}\left(\frac{\alpha_\mathrm{s}^2+\sigma^2}{\alpha_\mathrm{r}^2+\sigma^2}\right)^{1/4}=\frac{1}{\tau_\mathrm{r}}, \tag{59}$$

$$\mu_\mathrm{s}=\frac{1}{(\alpha_\mathrm{rs}\sigma)^{1/2}}\left(\frac{\alpha_\mathrm{r}^2+\sigma^2}{\alpha_\mathrm{s}^2+\sigma^2}\right)^{1/4}=\frac{1}{\tau_\mathrm{s}}, \tag{60}$$

#162929 - $15.00 USD Received 13 Feb 2012; revised 16 Mar 2012; accepted 16 Mar 2012; published 26 Mar 2012

where τ_j are the characteristic frequency-scales found in the frequency-domain Schmidt decomposition.

In the limit of short fibers $\beta l/\tau \to 0$ we find that

$$\lambda_0 \to (\gamma h l)^2 w/(4\sigma^2) = (\gamma h l)^2 w/(2\tau^2), \tag{61}$$

$$\mu_j \to 1/(\alpha_{\rm rs}\sigma)^{1/2} = 2^{1/4}/(\alpha_{\rm rs}\tau)^{1/2}. \tag{62}$$

The square of the Schmidt coefficient scales quadratically with the length and the characteristic time-scales are the geometric means of $\alpha_{\rm rs}$ and σ, and increase with the square root of the fiber length. In this limit the separability coefficient (denoted t in the appendix) tends to

$$\mu \to 1 - \alpha_{\rm rs}/\sigma, \tag{63}$$

which is close to unity, in other words this leads to a large number of non-zero Schmidt coefficients. In this limit of short fibers the sidebands experience approximately CW pumps when the pump-width is much larger than the sideband-width. Notice that the duration of the lowest-order Schmidt modes are much shorter than the pumps (it is the geometric mean of the transit time and the pump width). Also for signal-to-idler generation a pulse that is an arbitrary superposition of lower-order modes is converted without significant distortion, since the Schmidt coefficients decrease slowly as μ is close to unity.

For the other limit where $\beta l/\tau \to \infty$ we find

$$\lambda_0 \to (\gamma h)^2/|\beta_{\rm r}\beta_{\rm s}|, \tag{64}$$

$$\mu_{\rm r} \to (\alpha_{\rm s}/\alpha_{\rm r})^{1/2}/(\alpha_{\rm rs}\sigma)^{1/2}, \tag{65}$$

$$\mu_{\rm s} \to (\alpha_{\rm r}/\alpha_{\rm s})^{1/2}/(\alpha_{\rm rs}\sigma)^{1/2}. \tag{66}$$

The Schmidt coefficient tends to a constant, and the time-scales are now approximately the geometric mean of $\alpha_{\rm rs}$ and σ, and increase as the square root of the length. This is because the pumps overlap throughout the entire fiber. As discussed before; in this limit it is more reasonable to set $h = 1$ because the step-functions are almost equal to unity. The separability coefficient tends to

$$\mu \to 1 - \sigma\alpha_{\rm rs}/|\alpha_{\rm r}\alpha_{\rm s}|, \tag{67}$$

which is also close to unity. Thus, we would expect many Schmidt modes and therefore a non-separable Green function.

3.4. Numerical studies

Before we consider numerical studies of the various functions in this paper we discuss the natural dimensionless parameters to use. The efficiency of conversion is quantified by the dimensionless parameter $\overline{\gamma} = \gamma/\beta_{\rm rs}$, but this is not a parameter that is going to be varied since we consider the low-conversion efficiency limit which puts a natural limit on the conversion strength $\overline{\gamma} \ll 1$. The natural unit to measure time in is in units of the pump-width and similarly for the length parameter it is natural to use the pump-width divided by β. For the remainder of the paper it is assumed that $\beta_{\rm r} = \beta = -\beta_{\rm s}$ in the numerical studies, so $\beta_{\rm rs} = 2\beta$.

To better understand the implications of the step-functions and the Gaussian approximation several numerical studies were performed, see Fig. 4. In Figs. 4(a) and 4(b) the Green function is plotted in the time-domain with and without the Gaussian approximation for a short fiber $\beta l/\tau = 1$ and for the Gaussian approximation we choose $h = 1.28$. In this limit the Gaussian approximation gives a qualitative answer, but it is only moderately accurate. In Figs. 4(c) and 4(d) the two Green functions are plotted with the normalized fiber-length set such that it should

#162929 - $15.00 USD Received 13 Feb 2012; revised 16 Mar 2012; accepted 16 Mar 2012; published 26 Mar 2012

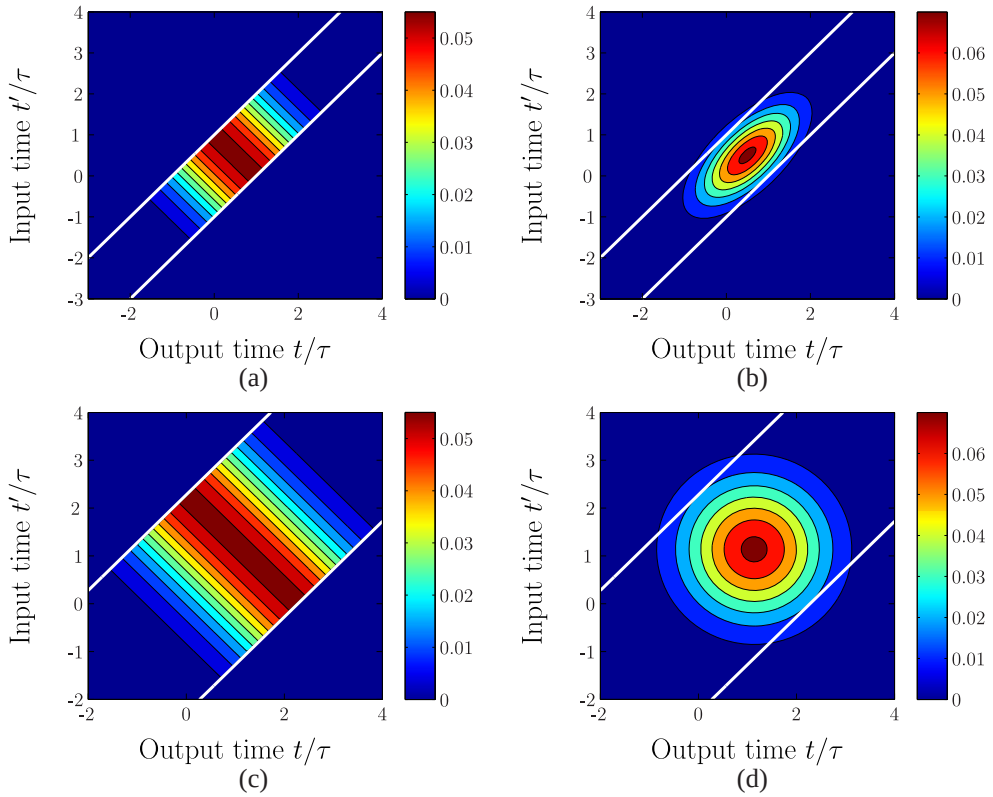

Fig. 4. Numerical studies of the Green function $G_{\rm rs}$. In all the plots $\beta = 1$, $\bar{\gamma} = 0.1$. The two pumps are normalized Gaussians with a root-mean-square width $\tau = 1$. The white lines denote the cut-off due to the step-functions, but they only apply to the Green functions without the Gaussian approximation. For the approximate Green functions the height $h = 1.28$ was used. (a) The absolute value of the step-function Green function for $\beta l/\tau = 1$, *i.e.* the non-separable case. (b) The Green function with the Gaussian approximation for $\beta l/\tau = 1$. (c) The absolute value of $G_{\rm rs}$ for $\beta l/\tau = 2.2768$, the case where it is expected to be separable. The shape of the function implies that no separability is attainable. (d) The Gaussian approximation for the separable fiber-length, and it is indeed seen to be separable.

#162929 - $15.00 USD Received 13 Feb 2012; revised 16 Mar 2012; accepted 16 Mar 2012; published 26 Mar 2012

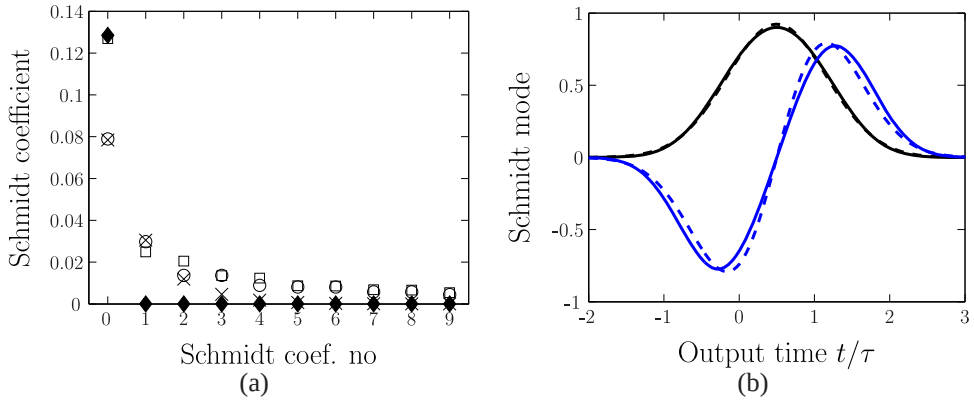

Fig. 5. (a) The Schmidt coefficients for the four plots in Fig. 4. Diamonds and crosses are for the separable and non-separable fiber length respectively with the Gaussian window whereas squares and open circles are the Schmidt coefficients with the rectangle window for the separable and non-separable length respectively. Notice that numerical study for the separable fiber-length, shows that the Gaussian approximation leads to separability, whereas the one with step-functions does not. (b) The first two Schmidt modes. The dashed curves are the Schmidt modes for the Gaussian Green function and the solid ones for the step-function window. The black curves are the zeroth-order modes and the blue curves the first-order modes. The normalized length of the fiber is one in this numerical study.

be separable. We remind the reader of the criterion for separability is $\alpha_r\alpha_s = -\sigma^2$, thus giving $\beta l/\tau = (2/w)^{1/2} \approx 2.2768$. By looking at the contour-plots it is clear that the Green function with the Gaussian approximation is clearly separable whereas the step-function Green function is not, as it is rotated with respect to the frequency axes. This hypothesis is confirmed in Fig. 5(a) where the Schmidt coefficients for the four Green functions are plotted. The Schmidt coefficients are determined by using the analytic form of the Green function for which the Schmidt decomposition is performed numerically. It gives qualitatively the same Schmidt coefficients for the non-separable fiber-length. For the separable fiber-length we have only one non-zero Schmidt coefficient with the Gaussian approximation, but several non-zero coefficients for the rectangular window. In Fig. 5(b) the first two Schmidt modes are compared for the two Green functions for the non-separable fiber-length. Again the qualitative behavior is the same, but it is only moderately accurate. In conclusion, the time-domain collision analysis does highlight new physics compared to the standard sinc/Gaussian approximation. The standard criteria for separability was seen to be an artifact from the approximation of the step-function with a Gaussian. Indeed for the non-convecting pumps the Green function is never completely separable for Gaussian pumps since they depend only on t_c^2 which includes both the input and the output times. However, the first Schmidt coefficient is 36 times larger than the next one, so the Green function is approximately separable.

Previously it was discussed that there was a discrepancy in the choice of the height of the approximating Gaussian in the case of short and long fibers. In Fig. 6(a) the first ten Schmidt coefficients are plotted for $h = 1$ and $h = 1.28$ for the Gaussian windows as well as the step-index window for a long fiber $\beta l/\tau$. Notice that none of the Green functions are separable, as discussed in the previous paragraph. Furthermore, neither of the Gaussian Green functions accurately represents the Green function with the rectangular window. This is because the Green function is constant along the $t - t'$ contours, such that the Green function always has a finite value at the cut-off lines. Figure 6(b) shows the two lowest-order Schmidt modes for this long

#162929 - $15.00 USD Received 13 Feb 2012; revised 16 Mar 2012; accepted 16 Mar 2012; published 26 Mar 2012

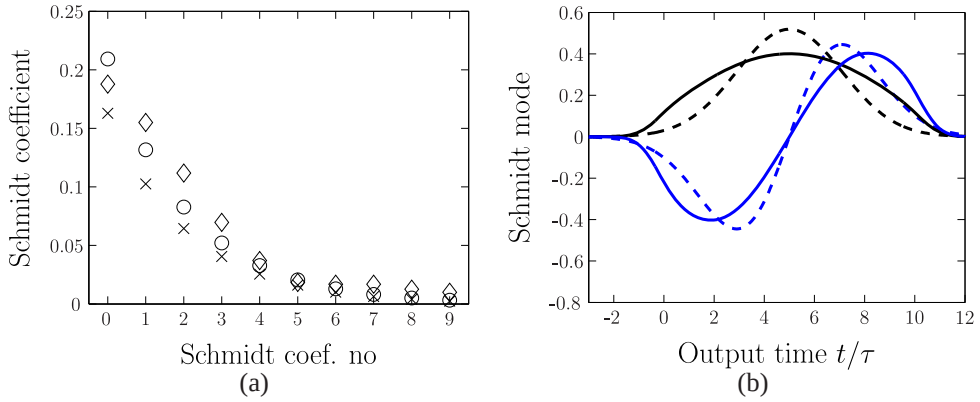

Fig. 6. (a) A plot of the Schmidt coefficients for a long fiber $\beta l/\tau = 10$. The crosses and circles are the Schmidt coefficients for the Gaussian window for $h = 1$ and $h = 1.28$ respectively. The diamonds are for the rectangular window. (b) The first two Schmidt modes. The dashed curves are the Schmidt modes for the Gaussian window while the step-function Schmidt modes are solid. Again the black curves are the zeroth-order modes and the blue curves the first-order modes. Notice that since the Schmidt modes are normalized they are identical for both heights in the Gaussian approximation.

fiber. Notice that since the Schmidt modes are normalized they are identical for the two different heights for the Gaussian window. In this case there is a large discrepancy between the Schmidt modes of the two different windows, thus reaffirming that replacing the rectangular function with the Gaussian is not always insignificant.

4. Convecting pumps

The results presented in the previous section gave physical insight into FC by BS. To improve the accuracy of the model we have to include the walk-off between the pumps since they have different group slownesses. As seen from Fig. 1, we treat the common case that the pumps and sidebands are placed pairwise symmetrically around the zero-dispersion frequency, which means that for closely and moderately spaced pumps and sidebands, pump p co-propagate with the signal and likewise pump q co-propagates with the idler, because the group-slowness is symmetrical around the zero-dispersion frequency. This approximation is valid for a wide range of experimental parameters and throughout the paper we assume that this is the case [34, 38]. Even when this assumption is not completely accurate, Eq. (46) is still valid, so it is easy to determine the accuracy of this approximation.

With the aforementioned assumption, the pumps are described by

$$A_{\mathrm{p}}(z,t) = F_{\mathrm{p}}[t - \beta_{\mathrm{s}}(z - z_{\mathrm{i}})], \tag{68}$$
$$A_{\mathrm{q}}(z,t) = F_{\mathrm{q}}[t - \beta_{\mathrm{r}}(z - z_{\mathrm{i}})], \tag{69}$$

where F_j are normalized shape-functions. The pumps intersect at the distance z_{i} in the fiber. With this pump ansatz, our coupling function γ_{pq} in G_{rs} depends on A_{p} and A_{q} which are functions of

$$t_{\mathrm{cr}} - \beta_{\mathrm{s}}(z_{\mathrm{cr}} - z_{\mathrm{i}}) = t' + \beta_{\mathrm{s}} z_{\mathrm{i}}, \tag{70}$$
$$t_{\mathrm{cr}} - \beta_{\mathrm{r}}(z_{\mathrm{cr}} - z_{\mathrm{i}}) = t - \beta_{\mathrm{r}}(l - z_{\mathrm{i}}), \tag{71}$$

#162929 - $15.00 USD Received 13 Feb 2012; revised 16 Mar 2012; accepted 16 Mar 2012; published 26 Mar 2012

respectively. Inserting these pumps in Eq. (46) leads to

$$G_{\rm rs}(t;t') = {\rm i}\bar{\gamma}A_{\rm q}^*[t-\beta_{\rm r}(l-z_{\rm i})]A_{\rm p}[t'+\beta_{\rm s}z_{\rm i}] \times {\rm H}(t'+\beta_{\rm r}l-t)\,{\rm H}(t-t'-\beta_{\rm s}l), \quad (72)$$

where $\bar{\gamma}=\gamma/|\beta_{\rm rs}|$. This Green function is naturally separable, and the input and output Schmidt modes are the shape functions of pumps p and q, respectively. Only the step-functions prevent complete separability, but for a sufficiently long fiber they are equal to unity for times of interest.

The other Green function was defined in Eq. (50) with the associated collision point defined in Eq. (49). Using the collision distance and time we find that

$$t_{\rm cs}-\beta_{\rm s}(z_{\rm cs}-z_{\rm i}) = t-\beta_{\rm s}(l-z_{\rm i}), \quad (73)$$

$$t_{\rm cs}-\beta_{\rm r}(z_{\rm cs}-z_{\rm i}) = t'+\beta_{\rm r}z_{\rm i}, \quad (74)$$

and, hence, that

$$G_{\rm sr}(t;t') = {\rm i}\bar{\gamma}A_{\rm p}^*[t-\beta_{\rm s}(l-z_{\rm i})]A_{\rm q}[t'+\beta_{\rm r}z_{\rm i}] \quad (75)$$

$$\times {\rm H}(t'+\beta_{\rm r}l-t)\,{\rm H}(t-t'-\beta_{\rm s}l). \quad (76)$$

Results (72) and (76) have remarkable consequences. For a sufficiently long fiber we have in the case of signal-to-idler conversion that the natural input signal mode has the shape of pump p whereas the output idler mode attains the shape of pump q. The two modes are centered on $\beta_{\rm s}(l-z_{\rm i})$ and $\beta_{\rm r}z_{\rm i}$ respectively. For idler-to-signal conversion the natural input idler has the shape of pump q and the output idler attains the shape of pump p. In both cases the input and output Schmidt modes are timed to arrive at the intersection point of the pumps, since this will be the point of maximal interaction.

4.1. Gaussian pumps of equal width

Assuming two Gaussian pumps with the same width and $z_{\rm i}=l/2$, the Green function attains the form

$$G_{\rm rs}(t;t') = \frac{{\rm i}\bar{\gamma}}{\sqrt{\pi}\tau}\exp\left[-\frac{(t-\beta_{\rm r}l/2)^2+(t'+\beta_{\rm s}l/2)^2}{2\tau^2}\right] \times {\rm H}(t'+\beta_{\rm r}l-t)\,{\rm H}(t-t'-\beta_{\rm s}l). \quad (77)$$

The consequences of this result are illustrated in Fig. 7. We notice that this function is clearly separable for $\beta l/\tau=3$ and we confirm that the output mode, the first Schmidt mode for $l=3$, indeed is a copy of pump q centered on $\beta_{\rm r}l/2$. It is difficult to conclude anything about the higher-order Schmidt modes, but a consequence of the Sturm comparison theorem, [52], is that the eigenfunctions of a Sturm-Liouville problem have a monotonically increasing number of zeros . Since the Schmidt modes are eigenfunctions of the integral equations [*cf.* Eqs. (97) and (98)] we expect them to show the same behavior, which is confirmed by Fig. 7(d).

To check the hypothesis that the optimal interaction distance was half that of the fiber, a numerical study was performed of the square of the first two Schmidt coefficients λ_0 and λ_1 as a function of the interaction distance for two different fiber lengths. The result is seen in Figure 8 which confirms that the strongest frequency conversion is at $z_{\rm i}=l/2$. An interesting result is that for the short fiber the first two Schmidt coefficients have maxima at $z_{\rm i}=l/2$, which shows that the two lowest-order Schmidt modes have the maximal conversion there. This result was not replicated for the longer fiber, where the second Schmidt coefficient have minima at $z_{\rm i}=l/2$, but this is because the Green function is separable and changing $z_{\rm i}$ moves the Green function in the (t,t') plane leading to a cut-off due to the step-functions.

#162929 - $15.00 USD Received 13 Feb 2012; revised 16 Mar 2012; accepted 16 Mar 2012; published 26 Mar 2012

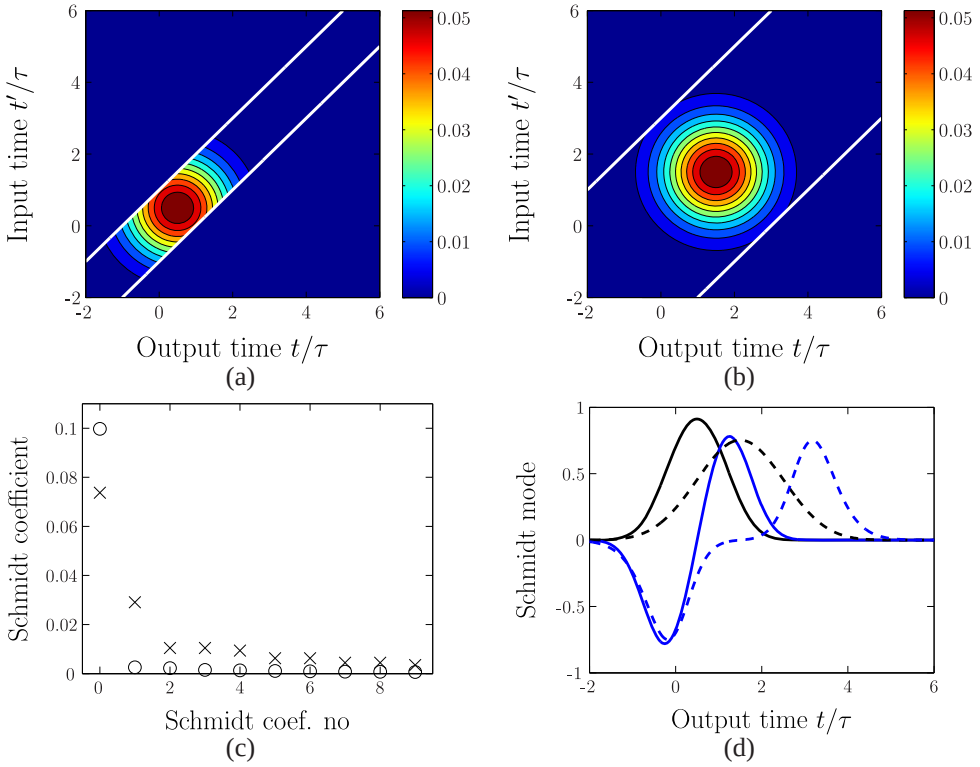

Fig. 7. Numerical studies of the Green function G_{rs} when including the convecting pumps. In all the plots $\beta_{\mathrm{r}} = 1 = -\beta_{\mathrm{s}}$, $\overline{\gamma} = 0.1$. The numerical study uses Gaussian pumps with a root-mean square width $\tau = 1$. In (a) and (b) white lines denote the cut-off due to the step-functions. (a) The absolute value of the Heaviside Green function for $\beta l/\tau = 1$. (b) The Green function for $\beta l/\tau = 3$. (c) A plot of the Schmidt coefficients for the two fiber lengths where the crosses are for the shorter length and the circles for $\beta l/\tau$. For $\beta l/\tau = 3$ the function is almost separable which is seen since we only have one dominating Schmidt mode. (d) The two first output Schmidt modes for the two lengths. The solid curves are for $\beta l/\tau = 1$ and the dashed ones for $\beta l/\tau = 3$. The lowest-order Schmidt mode is plotted in black and the next one in blue. For $\beta l/\tau = 3$ the first output mode corresponds to the shape of pump q centered on $\beta_{\mathrm{r}} l/2$ like expected. The second output mode has another shape, but its Schmidt coefficient is almost zero, so this mode is negligible.

#162929 - $15.00 USD Received 13 Feb 2012; revised 16 Mar 2012; accepted 16 Mar 2012; published 26 Mar 2012

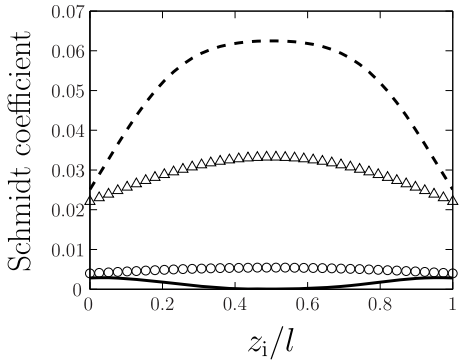

Fig. 8. The square of the first two Schmidt coefficients as a function of the interaction distance z_i. The triangles and circles correspond to λ_0 and λ_1 respectively for $\beta l/\tau = 1$. The dashed line is the square of the lowest-order Schmidt coefficient squared and the solid line the square of the next Schmidt coefficient for $\beta l/\tau = 3$.

4.1.1. The Gaussian approximation

To compare the results related to convecting Gaussian pumps with the ones found in the non-convecting case, once again the step-functions are approximated by a best-fit Gaussian, yielding

$$G_{\rm rs}(t;t') \approx \frac{i\overline{\gamma}h}{\pi^{1/2}\tau}\exp\left[-\frac{(\tau^2+\alpha_{\rm rs}^2)\overline{t}^2 - 2\tau^2\overline{t}\overline{t'} + (\tau^2+\alpha_{\rm rs}^2)(\overline{t'})^2}{2(\tau\alpha_{\rm rs})^2}\right], \tag{78}$$

where $\overline{t}$ and $\overline{t'}$ are the delayed and advanced output and input times respectively, h is the height fitting parameter, and $\xi = 0.3858$ is the constant that gives the same full-width half-maximum for the approximation of the sinc with a Gaussian. This expression clearly shows that the Green function is separable in the limit of long fibers since $\alpha_{\rm rs} \propto l$ and the cross-term is proportional to $1/\alpha_{\rm rs}^2$.

Comparing with Eq. (104) we note that the argument of Eq. (78) is of the same form, hence inserting from Eq. (78) and using Eq. (109) leads to

$$\lambda_0 = \frac{(\gamma h l)^2 w}{2[\alpha_{\rm rs}^2+\tau^2+\alpha_{\rm rs}(\alpha_{\rm rs}^2+2\tau^2)^{1/2}]}, \tag{79}$$

$$\mu_j = \frac{[\alpha_{\rm rs}^2(\alpha_{\rm rs}^2+2\tau^2)]^{1/4}}{\alpha_{\rm rs}\tau}, \tag{80}$$

$$\mu = \frac{\alpha_{\rm rs}^2+\tau^2-\alpha_{\rm rs}(\alpha_{\rm rs}^2+2\tau^2)^{1/2}}{\tau^2}, \tag{81}$$

where again μ_j has been used instead of τ_j to avoid confusion.

In the limit of short fibers ($\beta l/\tau \to 0$) corresponding to $\tau \gg \alpha_{\rm rs}$ we find

$$\lambda_0 \to (\gamma h l)^2 w/(2\tau^2), \tag{82}$$

$$\mu_j \to 2^{1/4}/(\alpha_{\rm rs}\tau)^{1/2} = 1/(\alpha_{\rm rs}\sigma)^{1/2}, \tag{83}$$

$$\mu \to 1-\alpha_{\rm rs}2^{1/2}/\tau = 1-\alpha_{\rm rs}/\sigma. \tag{84}$$

Notice that these results are the same we found for the non-convecting case, Eqs. (61)–(63), as expected since the effect of convection is imperceptible for short lengths. The square of the lowest-order Schmidt coefficient increases quadratically with length, a typical result from

#162929 - $15.00 USD Received 13 Feb 2012; revised 16 Mar 2012; accepted 16 Mar 2012; published 26 Mar 2012

coherent scattering processes. The time-scale of the Schmidt modes is simply the geometric mean of α_{rs} and σ, and increases as the square root of the length.

In the complementary limit in which $\beta l/\tau \to \infty$,

$$\lambda_0 \to (\gamma h)^2/\beta_{\mathrm{rs}}^2, \quad \mu_j \to 1/\tau, \quad \mu \to 0. \tag{85}$$

Thus the squared Schmidt coefficient tends to a constant (which is identical to the one found in the exact model for $h = 1$). Also the time-scale is simply the pump-width. Comparing with the non-convecting case, Eqs. (64)–(67), the lowest-order Schmidt coefficient in both cases tends to a constant, but the time-scales differ as they now tend to a constant whereas the non-convecting ones grow with the square root of the fiber-length. Also the separability parameter tends to zero, such that the Green function is always separable for sufficiently long fibers, which was not the case for the non-convecting model that was only separable under the Gaussian approximation and under specific conditions. This contrasts to the non-convecting model because the interaction for the convecting case happens only during the collision, leading to separability and the drop-out of the length dependence.

These limits were tested numerically for the convecting case, see Fig. 9(a). The figure shows the square of the lowest-order Schmidt coefficient for the Green functions with the Gaussian- and step-function windows. It is seen that the Gaussian window over-estimates the value of the Schmidt coefficient for long fibers, but setting $h = 1$, such that the Gaussian has the same height as the rectangular function gives a better agreement. This is reasonable, as the rectangular window for large fiber-lengths is approximately unity. In the short fiber limit the two models disagree for $h = 1$, but one is free to choose w to obtain better accuracy since the long-fiber limit, Eq. (85) is independent of w. The width of the best-fit Gaussian in the time-domain was determined by matching the FWHM in the frequency-domain of the Gaussian and the sinc function. However, the FWHM of the inverse Fourier transform is not necessarily the same. By choosing the width such that the Gaussian and the rectangle have the same FWHM in the time-domain, one finds $w = 0.7213$. The square of the Schmidt coefficients with this width is seen in Fig. 9(b). Choosing this width results in a better fit in the short fiber limit, than the result of the traditional sinc approximation. By fitting w to the Schmidt coefficients with the rectangular window using Eq. (79), we were able to find a slightly better fit for intermediate fiber lengths for $w \approx 0.86$, but at the cost of a worse fit for short fibers. Thus we conclude that the best fit is found for $h = 1$ and matching the FWHM in the time-domain.

4.2. Different Gaussian pumps

The next investigation considers Gaussian pumps with different widths. This leads to the Green function

$$G_{\mathrm{rs}}(t;t') = \frac{\mathrm{i}\bar{\gamma}}{(\pi\tau_{\mathrm{p}}\tau_{\mathrm{q}})^{1/2}} \exp\left[-\frac{(t-\beta_{\mathrm{r}}l/2)^2}{2\tau_{\mathrm{q}}^2} + \frac{(t'+\beta_{\mathrm{s}}l/2)^2}{2\tau_{\mathrm{p}}^2}\right] \times \mathrm{H}(t'+\beta_{\mathrm{r}}l-t)\,\mathrm{H}(t-t'-\beta_{\mathrm{s}}l), \tag{86}$$

for $z_{\mathrm{i}} = l/2$. This case is investigated in Fig. 10 for $\tau_{\mathrm{q}} = \tau_{\mathrm{p}}/2$. In (a) and (b) the Green function is plotted for $\beta l/\tau_{\mathrm{p}} = 1$ and 3 respectively. The function is clearly elongated in the t' direction because pump p is twice as broad. Fig. 10(c) shows the Schmidt coefficients for the two cases and for the longer fiber the function is definitely still separable in spite of the different pump widths. This agrees with the hypothesis since it is only the step-functions that prevent separability and as long as the ridge is wider than the pump-widths the Schmidt decomposition should only contain one term. The shorter fiber has a slightly larger lowest-order Schmidt coefficient compared to Fig. 10(c) resulting in a larger degree of separability because the higher-order

#162929 - $15.00 USD Received 13 Feb 2012; revised 16 Mar 2012; accepted 16 Mar 2012; published 26 Mar 2012

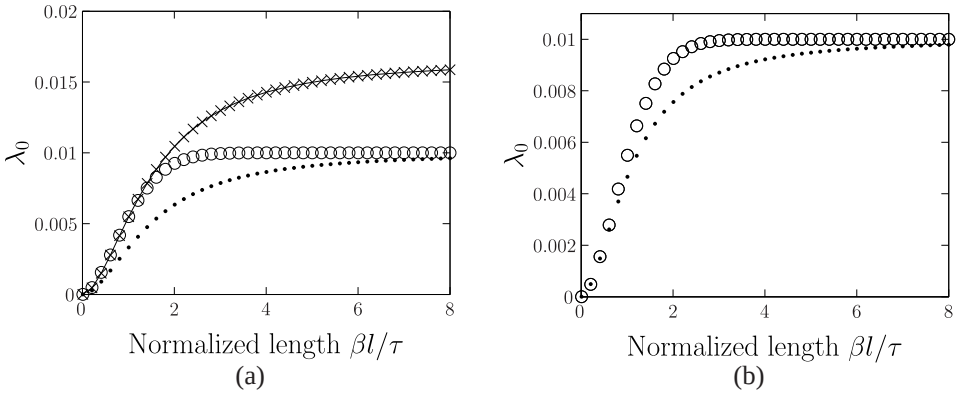

Fig. 9. Plots of the square of the lowest-order Schmidt coefficient as a function of the length of the fiber. (a) For $w = \xi = 0.3858$, the value giving the same FWHM in the frequency-domain. The solid line is the square of the analytic lowest-order Schmidt coefficient, Eq. (79) with $h = [2/(w\pi)]^{1/2} \approx 1.28$. The crosses are the numerically found values for the Gaussian approximated Green function, which agrees with the analytic value. The open circles are also found numerically, but are for the convecting Green function with step-function window. Finally the dots is Eq. (79) with $h = 1$. (b) The same curves as the left panel but for $h = 1$ and $w = 0.7213$ which is the width giving the same FWHM in the time-domain.

Schmidt coefficients are smaller. This is because the pulse is narrower in one direction and thus less of the Green function is exposed to the sharp boundaries. In Fig. 10(d) the two lowest output modes for the different fiber lengths are shown. As expected the lowest-order mode for the separable state is simply a copy of pump q centered on $\beta l/\tau = 1/2$ [*cf.* Eq. (72)], whereas the lowest-order mode for the shorter fiber is distorted, because the step-functions are not negligible in this case.

The lowest-order Schmidt coefficient was also considered for various aspect ratios, see Fig. 11(a). As the aspect ratio increases for a constant length the coefficient falls off since the value of the Green-function at the cut-off points increases, and it is therefore less separable. However, if the length increases with the aspect ratio it is possible to achieve separability over a wide range of aspect ratios. This is expected since in this case where pump q is wide compared to p and thus sideband r is wide and s narrow, for a long enough fiber the two short pulses propagate past the longer ones and hence experience a full collision [53].

For quantum communication it is of interest to convert the states emitted from a quantum memory unit to a shape suitable for transmission in an optical communication system. This might include reshaping the pulse width by a factor of 100 [13]. To check whether such a reshaping is possible within the perturbative framework, a numerical study with $\tau_q = \tau_p/100$ was carried out with the Schmidt coefficients in Fig. 11(b). This definitely shows that the Green function for the longer fiber lengths is separable, but this is a natural extension of the discussion in Fig. 10(c).

4.2.1. The Gaussian approximation

In a similar way as the analysis for the Green function with two identical Gaussian pumps we are interested in investigating the effect of the Gaussian approximation. Two different pump-widths corresponds to replacing τ with $(\tau_p\tau_q)^{1/2}$, and τ_q and τ_p in front of $\bar{t}$ and $\bar{t}'$ respectively, in Eq. (78). For the limit where the aspect ratio tends to infinity or in other words $\tau_p \to 0$ and

#162929 - $15.00 USD Received 13 Feb 2012; revised 16 Mar 2012; accepted 16 Mar 2012; published 26 Mar 2012

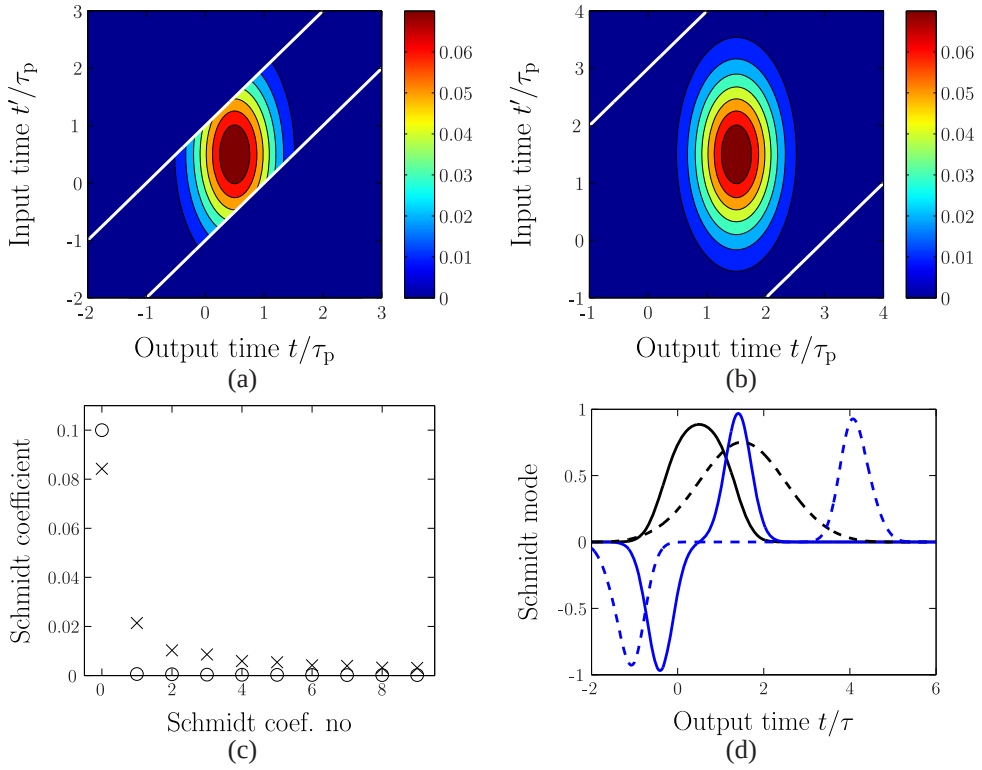

Fig. 10. Plots of the Green function G_{rs} with different pump widths in this case $\tau_q = \tau_p/2$. In (a) $\beta l/\tau_p = 1$ whereas (b) considers $\beta l/\tau_p = 3$. The function is elongated in the t' direction since pump p has the largest width. (c) shows the Schmidt coefficients where open circles are for the longer fiber-length. The long fiber Green function is still separable even though the pumps have different widths. In (d) the two lowest-order Schmidt modes for the two lengths is plotted. The black curves are the lowest-order Schmidt mode and the blue ones the next one. Dashed curves are for the longer fiber.

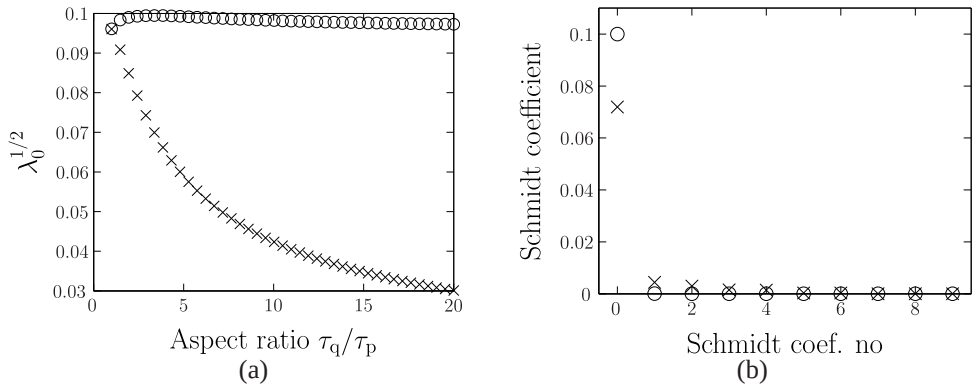

Fig. 11. Plot of the lowest-order Schmidt coefficient as a function of the aspect ratio. The crosses are for $\beta l/\tau_p = 2$ and the open circles for the variable length $2\tau_q/\tau_p$. (b) The Schmidt coefficients for a pulse with a very narrow aspect ratio ($\tau_q = \tau_p/100$) for two different fiber lengths $\beta l/\tau_p = 0.5$ (crosses) and 3 (open circles)

.

#162929 - $15.00 USD Received 13 Feb 2012; revised 16 Mar 2012; accepted 16 Mar 2012; published 26 Mar 2012

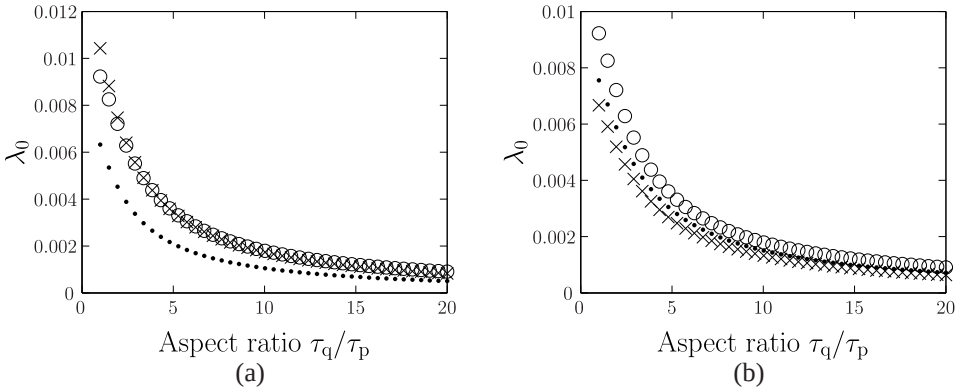

Fig. 12. Plots of the limits of the square of the lowest-order Schmidt coefficient as a function of the aspect ratio. (a) This figure shows convecting pumps where $\beta l/\tau_p = 2$, $w = 0.3858$ and the open circles are for the rectangular windows and filled circles and crosses are for the Gaussian window with $h = 1$ and $h = 1.28$ respectively. (b) The same functions as the left panel but for the the width yielding the same FWHM in the time-domain, $w = 0.7213$.

$\tau_q \to \infty$ we find that

$$\lambda_0 \to (\gamma h/\beta_{rs})^2(\alpha_{rs}/\tau_q), \quad \mu_r \to 1/\alpha_{rs}, \quad \mu_s \to 1/\tau_p. \tag{87}$$

Notice that the two time-scales are no longer identical, as expected, and they are determined by the smaller of either α_{rs} or τ_j. The square of the Schmidt coefficient differs from $\overline{\gamma}^2$ by the factor α_{rs}/τ_q.

These results were simulated, see Fig. 12(a). In general, the Gaussian window with $h = 1$ underestimates the lowest-order Schmidt coefficient, but for large aspect ratios the lower window height approximates the right result. Also the lowest-order Schmidt coefficients fall off since the length of the fiber was held constant. In the right panel the square of the lowest-order Schmidt coefficient is plotted for $w = 0.7213$. In this case the lower window height does give a better approximation, but it is only moderately accurate. This is because the Green function has a large value at the cut-off which makes the Gaussian approximation a less accurate fit.

4.3. HG0/HG1 pumps

Next we consider the case with a Hermite-Gaussian (HG) temporal shape of the pump of zeroth order (HG0, a Gaussian) for pump p, and a HG pump of first order, HG1, for pump q. The results are plotted in Fig. 13. Since the HG1 profile is slightly wider a longer fiber was used for the long-fiber case ($\beta l/\tau = 4$). Again separability is indeed possible for the long fiber as seen from the fact that the second coefficient is almost zero in Fig. 13(c). From Eq. (72) it is expected that the output mode corresponds to that of pump q centered on $l/2$ for a sufficiently long fiber where the step-functions are negligible. Since pump q in this case is HG1 it is expected that the output mode will also be HG1 which is confirmed for $\beta l/\tau = 4$ in Fig. 13(d) the zeroth-order output mode is a HG1 centered on $l/2$. The zeroth-order mode for the shorter fiber is a distorted HG1 function centered also on $l/2$.

#162929 - $15.00 USD Received 13 Feb 2012; revised 16 Mar 2012; accepted 16 Mar 2012; published 26 Mar 2012

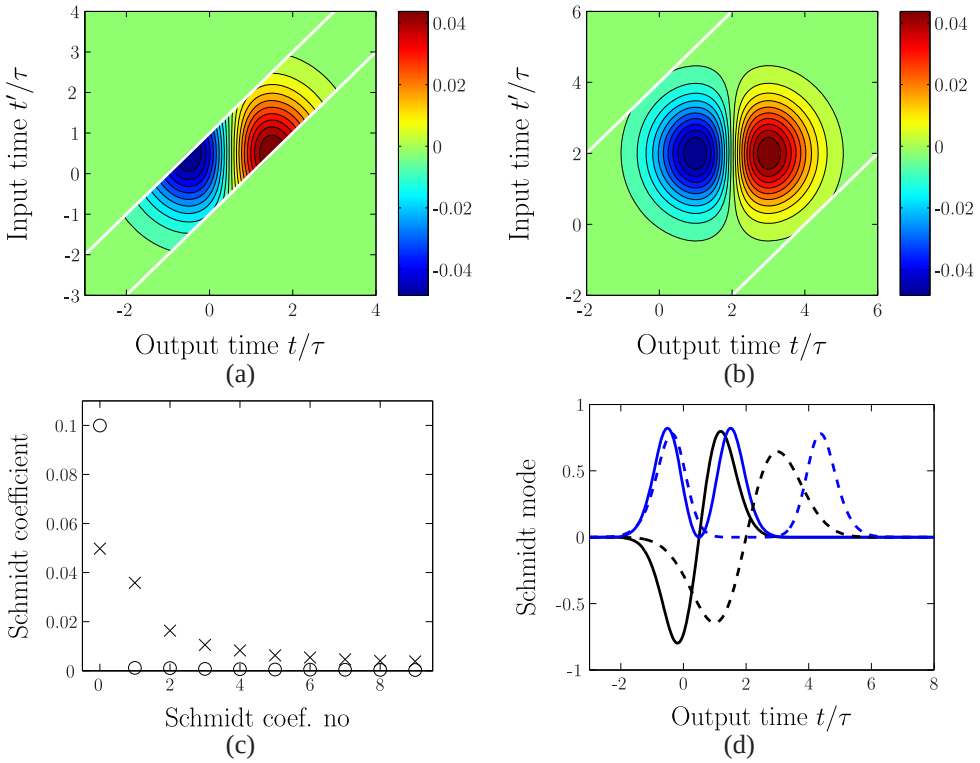

Fig. 13. Numerical study of the Green function $G_{\rm rs}$ with pump p as HG0 and pump q as HG1. In all the cases $\overline{\gamma} = 0.1$. (a) A plot of the Green function for $\beta l/\tau = 1$. (b) The Green function for the long fiber interaction, $\beta l/\tau = 4$. (c) The first 10 Schmidt coefficients for the two fiber lengths, where the open circles are for the longer case. The longer one is clearly separable. (d) The first two output Schmidt modes for each of the numerical studies, again black is for the lowest-order mode and blue for the next one, while dashed curves are the ones for the longer fiber. The long fiber first-order Schmidt mode is a HG1 centered on $\beta l/\tau = 2$ like expected, whereas the one for the shorter fiber is slightly distorted.

#162929 - $15.00 USD Received 13 Feb 2012; revised 16 Mar 2012; accepted 16 Mar 2012; published 26 Mar 2012

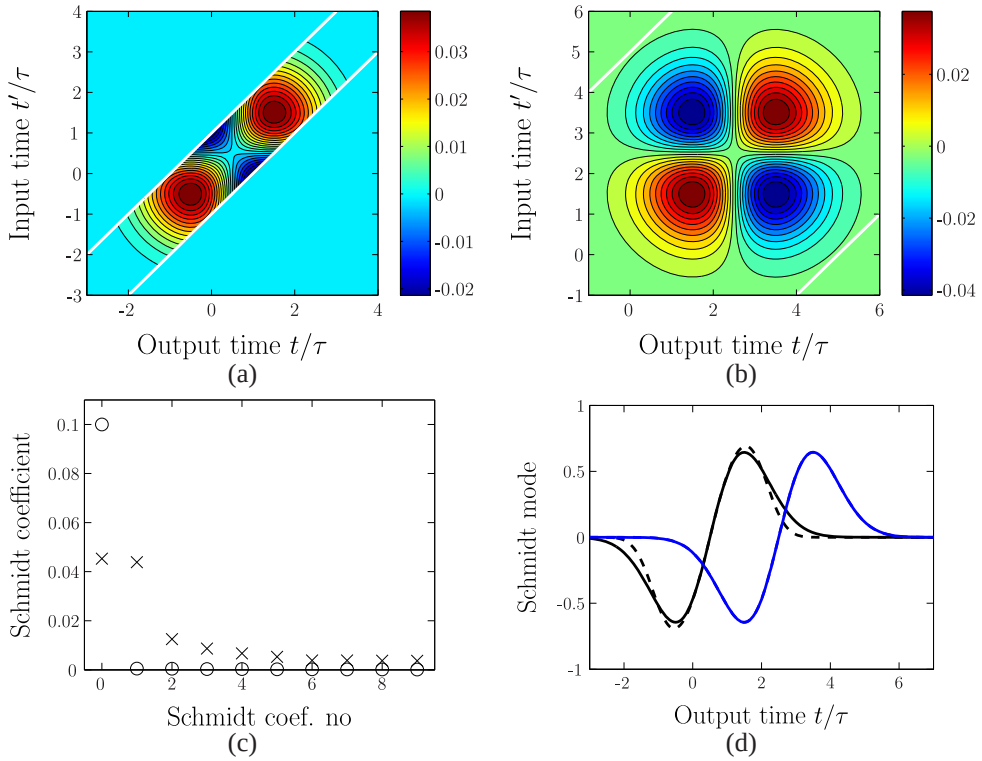

Fig. 14. Plots of the Green function $G_{\rm rs}$ where both pumps are HG1 functions and $\bar{\gamma} = 0.1$. (a) A contour plot of the Green function for the fiber length $\beta l/\tau = 1$. (b) The contour plot, for $\beta l/\tau = 5$. (c) The computed first 10 Schmidt coefficients for the two fiber lengths, open circles are again for the longer fiber which is clearly separable. (d) A plot of the lowest-order output Schmidt mode as well as the theoretical HG1 modes. The black curves are for the shorter fiber and the dashed curves are the numerically found Schmidt modes. The input modes have not been plotted since they coincided (as expected) with the output modes.

4.4. HG1/HG1 pumps

The final case considered is two identical HG1 pumps. Due to the larger width of the HG1 pumps, we consider $\beta l/\tau = 5$ to ensure separability. The result is seen in Fig. 14. From Fig. 14(b) and (c) it is clear that the Green function is separable for a sufficiently long fiber, which is expected. Considering Eq. (72), we expect the output and input modes for the separable case simply to be copies of the two pumps. This is indeed confirmed from Fig. 14(d) where the HG1 pumps coincide with the lowest-order input and output Schmidt mode (only the output mode has been plotted here since it was indistinguishable from the input mode). Again the shorter fiber leads to a slightly distorted HG1 mode. With this study we showed that FC is possible for relatively short fibers and more complicated pump-shapes.

5. Conclusion

In this paper we considered quantum-state preserving frequency conversion in both the frequency- and the time-domain using a perturbative analysis that is valid for low conversion efficiencies. The theoretical foundation was discussed and the Green function formalism introduced. The Schmidt decomposition was used as a useful tool to discuss separability and the

#162929 - $15.00 USD Received 13 Feb 2012; revised 16 Mar 2012; accepted 16 Mar 2012; published 26 Mar 2012

temporal modes comprising the Green functions. The Schmidt modes of the Green function are the natural input and output modes of the process. Next the Green functions were obtained in the frequency-domain in the low-conversion limit for stationary pumps that do not convect with respect to each other. The stationary model is a simplification of four-wave mixing but it is realistic for three-wave mixing where there is only one pump. The results were obtained using a standard analysis that assumes Gaussian pumps and the approximation of the system's sinc-function response by a best-fit Gaussian. The standard result was inverse Fourier transformed to the time-domain. Using the time-domain collision method, the solution was found in the time-domain for arbitrary pump-shapes and the effects of the assumptions made in the standard analysis were discussed. It was shown that for relatively stationary pumps complete separability is never possible for Gaussian pumps, and the conditions found using the standard model are artifacts of the sinc/Gaussian approximation. However the Green functions are close to being separable, and the predictions of the standard theory are reasonable in practice.

The collision method was generalized to also include convecting pumps. The Schmidt decomposition was used to find the natural modes of the problem and obtain important limits that allowed us to compare the stationary and the convecting models. In the short-fiber limit the predictions of the two models agree. It was also shown that convecting pumps allow for separable Green functions for sufficiently long fibers. This is in contrast to the stationary result that is only separable for one specific length. Additionally, we showed that it is possible to obtain arbitrary reshaping of a signal by a proper selection of the pump pulses. This was confirmed for simple Gaussian pumps and was also shown to be possible for two Gaussian pumps with very different widths. Finally higher-order Hermite-Gaussian shapes were also seen to allow for separability and reshaping. Preliminary numerical results show that reshaping also occurs in the high-conversion regime.

These results show that frequency conversion by four-wave mixing is a valuable resource for quantum information systems, as an convenient and reliable source for reshaping and frequency conversion, both of which are paramount for these systems to be used in practice. The low-conversion analysis will be extended to the high-conversion regime in future work.

A. Appendix: Mehler identity and kernel decomposition

Decompositions of Gaussian kernels are made possible by the Mehler identity [54, 55]

$$\exp\left[-\frac{t^2(x^2+y^2)}{(1-t^2)}+\frac{2txy}{(1-t^2)}\right]=(1-t^2)^{1/2}\sum_{n=0}^{\infty}\frac{t^n}{2^n n!}H_n(x)H_n(y), \tag{88}$$

where the Hermite polynomial

$$H_n(x)=\mathrm{e}^{x^2}(-\mathrm{d}_x)^n\mathrm{e}^{-x^2} \tag{89}$$

$$=\mathrm{e}^{x^2}\int_{-\infty}^{\infty}(2\mathrm{i}k)^n\mathrm{e}^{-k^2-2\mathrm{i}kx}\,\mathrm{d}k/\pi^{1/2}. \tag{90}$$

#162929 - $15.00 USD Received 13 Feb 2012; revised 16 Mar 2012; accepted 16 Mar 2012; published 26 Mar 2012

It follows from the integral representation (90) that

$$\begin{aligned}\sum_{n=0}^{\infty}\frac{t^n}{2^n n!}H_n(x)H_n(y) &= \frac{\mathrm{e}^{x^2+y^2}}{\pi}\iint_{-\infty}^{\infty}\sum_{n=0}^{\infty}\frac{(-2tkl)^n}{n!}\,\mathrm{e}^{-k^2-2\mathrm{i}xk}\mathrm{e}^{-l^2-2\mathrm{i}yl}\,\mathrm{d}k\mathrm{d}l\\ &= \frac{\mathrm{e}^{x^2+y^2}}{\pi}\iint_{-\infty}^{\infty}\mathrm{e}^{-k^2-2(tl+\mathrm{i}x)k}\mathrm{e}^{-l^2-2\mathrm{i}yl}\,\mathrm{d}k\mathrm{d}l\\ &= \frac{\mathrm{e}^{y^2}}{\pi^{1/2}}\int_{-\infty}^{\infty}\mathrm{e}^{-(1-t^2)l^2-2\mathrm{i}(y-tx)l}\,\mathrm{d}l\\ &= \frac{1}{(1-t^2)^{1/2}}\exp\left[-\frac{t^2(x^2+y^2)}{1-t^2}+\frac{2txy}{1-t^2}\right],\end{aligned} \tag{91}$$

which proves identity (88). By multiplying this identity by $\exp[-(x^2+y^2)/2]$, one obtains the related identity

$$\exp\left[-\frac{(1+t^2)(x^2+y^2)}{2(1-t^2)}+\frac{2txy}{(1-t^2)}\right] = [\pi(1-t^2)]^{1/2}\sum_{n=0}^{\infty}t^n\psi_n(x)\psi_n(y), \tag{92}$$

where the (orthonormal) Hermite functions

$$\psi_n(x) = \frac{H_n(x)\exp(-x^2/2)}{\pi^{1/4}(2^n n!)^{1/2}}. \tag{93}$$

The Schmidt decomposition theorem [56, 57] states that a complex kernel $K(x,y)$ may be written as the series

$$K(x,y) = \sum_{n=0}^{\infty}\lambda_n^{1/2}v_n(x)u_n^*(y). \tag{94}$$

The (non-negative) singular values λ_n are the (common) eigenvalues of the integral equations

$$\lambda u(x) = L_u u(x), \tag{95}$$

$$\lambda v(x) = L_v v(x), \tag{96}$$

where the hermitian (and non-negative) kernels are

$$L_u(x,x') = \int_{-\infty}^{\infty}K^*(x'',x)K(x'',x')\,\mathrm{d}x'', \tag{97}$$

$$L_v(x,x') = \int_{-\infty}^{\infty}K(x,x'')K^*(x',x'')\,\mathrm{d}x'', \tag{98}$$

and the associated eigenfunctions u and v satisfy the orthonormality relations

$$\int_{-\infty}^{\infty}u_m(x)u_n^*(x)dx = \delta_{mn} = \int_{-\infty}^{\infty}v_m(x)v_n^*(x)dx. \tag{99}$$

If K is real and symmetric, u and v are real and $L_u = L_v$.

Suppose that

$$K(x,y) = \exp\left[-\frac{(1+t^2)(x^2+y^2)}{2(1-t^2)}+\frac{2txy}{(1-t^2)}\right]. \tag{100}$$

Then the (common) hermitian kernel

$$L(x,y) = \left[\frac{\pi(1-t^2)}{(1+t^2)}\right]^{1/2}\exp\left[-\frac{(1+t^4)(x^2+y^2)}{2(1-t^4)}+\frac{2t^2xy}{(1-t^4)}\right]. \tag{101}$$

#162929 - $15.00 USD Received 13 Feb 2012; revised 16 Mar 2012; accepted 16 Mar 2012; published 26 Mar 2012

It follows from Eqs. (92) and (101) that

$$L(x,y) = \pi(1-t^2)\sum_{n=0}^{\infty} t^{2n}\psi_n(x)\psi_n(y). \tag{102}$$

Hence, the eigenfunctions that appear in decomposition (94) are the Hermite functions $\psi_n(x)$, and the eigenvalues

$$\lambda_n = \pi(1-t^2)t^{2n}. \tag{103}$$

These results also follow directly from Eqs. (92) and (100).

For asymmetrically-pumped FC,

$$K(\omega_\mathrm{r},\omega_\mathrm{s}) = \exp[-(a\omega_\mathrm{r}^2 + 2b\omega_\mathrm{r}\omega_\mathrm{s} + c\omega_\mathrm{s}^2)/2], \tag{104}$$

where a, c and $ac-b^2$ are all non-negative. One can rewrite Eq. (104) in the form of Eq. (100) by defining

$$t = -[(ac)^{1/2} - (ac-b^2)^{1/2}]/b, \tag{105}$$

$x = \tau_\mathrm{r}\omega_\mathrm{r}$ and $y = \tau_\mathrm{s}\omega_\mathrm{s}$, where

$$\tau_\mathrm{r} = [a(ac-b^2)/c]^{1/4}, \tag{106}$$

$$\tau_\mathrm{s} = [c(ac-b^2)/a]^{1/4}. \tag{107}$$

[The choice of root in Eq. (105) is determined by the requirement that $t \to 0$ as $b \to 0$]. The result is

$$\begin{aligned} K(\omega_\mathrm{r},\omega_\mathrm{s}) &= \sum_{n=0}^{\infty} \lambda_n^{1/2}\psi_n(\tau_\mathrm{r}\omega_\mathrm{r})\psi_n(\tau_\mathrm{s}\omega_\mathrm{s}) \\ &= \sum_{n=0}^{\infty} (\lambda_n/\tau_\mathrm{r}\tau_\mathrm{s})^{1/2}\tau_\mathrm{r}^{1/2}\psi_n(\tau_\mathrm{r}\omega_\mathrm{r})\tau_\mathrm{s}^{1/2}\psi_n(\tau_\mathrm{s}\omega_\mathrm{s}), \end{aligned} \tag{108}$$

where the singular values are specified by Eqs. (103) and (105), and the eigenfunctions $\tau_j^{1/2}\psi_n(\tau_j\omega_j)$ are normalized. If b is positive, t is negative and vice versa. However, the Hermite functions Eq. (93) do not depend on t and the singular values depend only on t^2, so Eqs. (103) and (108) omit sign information as written. One can restore this information by replacing t with $|t|$ and multiplying τ_r or τ_s by $s_c = -\,\mathrm{sign}(c)$. This change is equivalent to changing the sign of x or y in Eq. (100). By combining Eqs. (105)–(107), one can show that

$$\frac{\pi(1-t^2)}{\tau_\mathrm{r}\tau_\mathrm{s}} = \frac{2\pi}{(ac)^{1/2} + (ac-b^2)^{1/2}}, \tag{109}$$

This term appears in the formula for the Schmidt coefficients associated with normalized eigenfunctions.

For reference, the Fourier transform of a Hermite function is also a Hermite function. This result is a consequence of the fact that the Hermite functions are eigenstates of the harmonic-oscillator Hamiltonian, which is symmetric with respect to the position and momentum operators. One can prove this by multiplying the Hermite generating function [55] by $\exp(-x^2/2)$, to obtain the identity

$$\exp(-t^2 + 2tx - x^2/2) = \sum_{n=0}^{\infty} \frac{t^n}{n!}H_n(x)\exp(-x^2/2). \tag{110}$$

#162929 - $15.00 USD Received 13 Feb 2012; revised 16 Mar 2012; accepted 16 Mar 2012; published 26 Mar 2012

By Fourier transforming both sides of Eq. (110), according to the conventions

$$F(k) = (2\pi)^{-1/2} \int_{-\infty}^{\infty} F(x) \exp(-\mathrm{i}kx)\, \mathrm{d}x, \tag{111}$$

$$F(x) = (2\pi)^{1/2} \int_{-\infty}^{\infty} F(x) \exp(\mathrm{i}kx)\, \mathrm{d}x, \tag{112}$$

one obtains the transformed identity

$$\begin{aligned} &\sum_{n=0}^{\infty} \frac{t^n}{n!} \int_{-\infty}^{\infty} H_n(x) \exp(-x^2/2) \exp(-\mathrm{i}kx)\, \mathrm{d}x/(2\pi)^{1/2} \\ &= \exp[-(-\mathrm{i}t)^2 + 2(-\mathrm{i}t)k - k^2/2] \\ &= \sum_{n=0}^{\infty} \frac{(-\mathrm{i}t)^n}{n!} H_n(k) \exp(-k^2/2). \end{aligned} \tag{113}$$

By equating the coefficients of t^n in Eq. (113), one finds that

$$\int_{-\infty}^{\infty} \psi_n(x) \exp(-\mathrm{i}kx)\, \mathrm{d}x/(2\pi)^{1/2} = (-\mathrm{i})^n \psi_n(k), \tag{114}$$

where ψ_n was defined in Eq. (93). Hence, if the sideband wavepackets can be expressed as sums of frequency-domain Hermite functions, they can be expressed as related sums of time-domain Hermite functions.

The kernel was decomposed in the frequency-domain and the Schmidt modes were Fourier-transformed to the time-domain. Alternatively one can inverse-transform the kernel directly to the time-domain and then decompose it. To be able to compare the result in the time-domain with what we obtained in the frequency domain we consider the generalized Gaussian in the frequency-domain

$$F(\omega_\mathrm{r}, -\omega_\mathrm{s}) = \exp\left[-(a\omega_\mathrm{r}^2 + 2b\omega_\mathrm{r}\omega_\mathrm{s} + c\omega_\mathrm{s}^2)/2\right]. \tag{115}$$

By doing the requisite integrals explicitly, one can show that

$$F(t,t') = \exp\left[-\frac{ct_\mathrm{r}^2 + 2bt_\mathrm{r}t_\mathrm{s} + at_\mathrm{s}^2}{2(ac-b^2)}\right] / (ac-b^2)^{1/2}, \tag{116}$$

which is valid for a and c positive and $ac - b^2 > 0$. Equations (115) and (116) comprise a specific example of the general transform relation

$$\exp(-X^\mathrm{t} M X/2) \leftrightarrow \exp(-K^\mathrm{t} M^{-1} K/2)/[\det(M)]^{1/2}, \tag{117}$$

M is a symmetric matrix, X and K are column vectors, and the superscript t denotes a transpose. Formula (117) is a standard result. It is proved in Appendix A of [58].

Comparing with Eqs. (105)–(107) the time-domain kernel has an analytic Schmidt decomposition as it is in the canonical form. It has the same Schmidt-coefficients but the characteristic time-scales are $1/\tau_\mathrm{r}$ and $1/\tau_\mathrm{s}$ respectively. The time-domain Schmidt-modes are indeed Hermite functions, as stated previously.

Acknowledgments

MR was supported by the National Science Foundation, EPDT.

#162929 - $15.00 USD Received 13 Feb 2012; revised 16 Mar 2012; accepted 16 Mar 2012; published 26 Mar 2012